© 2016. Published by The Company of Biologists Ltd | Development (2016) 143, 1375-1387 doi:10.1242/dev.131276

RESEARCH ARTICLE

Influence of ovarian muscle contraction and oocyte growth on egg chamber elongation in *Drosophila*

Darcy Andersen and Sally Horne-Badovinac*

ABSTRACT

Organs are formed from multiple cell types that make distinct contributions to their shape. The *Drosophila* egg chamber provides a tractable model to dissect such contributions during morphogenesis. Egg chambers consist of 16 germ cells (GCs) surrounded by a somatic epithelium. Initially spherical, these structures elongate as they mature. This morphogenesis is thought to occur through a 'molecular corset' mechanism, whereby structural elements within the epithelium become circumferentially organized perpendicular to the elongation axis and resist the expansive growth of the GCs to promote elongation. Whether this epithelial organization provides the hypothesized constraining force has been difficult to discern, however, and a role for GC growth has not been demonstrated. Here, we provide evidence for this mechanism by altering the contractile activity of the tubular muscle sheath that surrounds developing egg chambers. Muscle hypo-contraction indirectly reduces GC growth and shortens the egg, which demonstrates the necessity of GC growth for elongation. Conversely, muscle hyper-contraction enhances the elongation program. Although this is an abnormal function for this muscle, this observation suggests that a corset-like force from the egg chamber's exterior could promote its lengthening. These findings highlight how physical contributions from several cell types are integrated to shape an organ.

KEY WORDS: *Drosophila*, Egg chamber, Morphogenesis, Muscular dystrophy, Laminin, Vitellogenesis

INTRODUCTION

When studying morphogenesis, it can often be difficult to tease apart the physical contributions that different cell types make to the form of a tissue or organ. The elongation of the *Drosophila* egg chamber provides an elegant system wherein these diverse contributions can be explored (Horne-Badovinac, 2014). The egg chamber is an organ-like structure within the ovary that will produce one egg. It is composed of a cluster of 16 interconnected germ cells, with one oocyte and 15 nurse cells, surrounded by a somatic epithelium of follicle cells. The follicle cells produce a basement membrane (BM) that forms this structure's outermost layer. Egg chambers are assembled near the ovary's anterior in the germarium and, once formed, join an array of 6-8 progressively older egg chambers. Together, the germarium and its associated egg chambers comprise one ovariole (Fig. 1A,B). Each egg chamber passes though 14 developmental stages. Although initially spherical, between stages 5 and 10 it lengthens along its anterior-posterior (AP) to create the elliptical shape of the egg.

Department of Molecular Genetics and Cell Biology, The University of Chicago, 920 East 58th Street, Chicago, IL 60637, USA.

*Author for correspondence (shorne@uchicago.edu)

Received 25 September 2015; Accepted 18 February 2016

Egg chamber elongation is thought to occur through a 'molecular corset' mechanism (Fig. S1A). The corset itself is provided by the follicular epithelium. Here, parallel arrays of actin bundles at each cell's basal surface and fibril-like structures in the adjacent BM all become aligned perpendicular to the elongation axis, a process that depends on rotation of the egg chamber within the BM (Cetera et al., 2014; Haigo and Bilder, 2011). Given the epithelium's closed topology, tissue-level organization of these structures produces a circumferential corset-like pattern around the egg chamber's exterior. Importantly, mutations that disrupt this pattern produce rounded eggs (Gates, 2012). These observations have led to the hypothesis that the actin bundles and BM fibrils provide an anisotropic constraining force that promotes elongation; however, whether such a force actually contributes to this morphogenesis has been difficult to discern.

The molecular corset model also posits a central role for germ cell growth in egg chamber elongation. Although the germ cells stop dividing before being encapsulated by the follicle cells, the cluster increases in volume through the end of stage 10 (stage 10b). The nurse cells increase their volumes throughout stages 1 to 10b, primarily through endoreplication of their genomes. By contrast, the oocyte undergoes an independent expansion beginning at stage 8 when it takes up yolk proteins, a process known as vitellogenesis (Bownes, 1982). These changes in germ cell volume are thought to create an internal pressure that is resisted by the epithelial corset to preferentially channel egg chamber growth along the AP axis. To date, however, a role for germ cell growth in the elongation program has not been demonstrated.

In addition to exploring the molecular corset model, this paper will introduce a role for ovarian muscles in egg chamber elongation. There are two muscle types in the ovary proper: (1) the epithelial sheath, a tube of muscle that surrounds each ovariole, and (2) the peritoneal sheath, a thin meshwork that surrounds the entire ovary (Hudson et al., 2008). We focus on the epithelial sheath, but will refer to this tissue as the 'muscle sheath' to avoid confusion with the follicular epithelial cells. Unlike the intestine, where the surrounding muscles are attached to the basal epithelial surface, the egg chambers slide relatively freely within the muscle sheath, which allows its rhythmic contractions to slowly propel them toward the oviduct. In this way, the muscle sheath functions similarly to smooth muscle; yet, it is striated like skeletal muscle. Given that the muscle sheath's circular fibers are primarily oriented perpendicular the egg chambers' AP axes, like the molecular corset (Fig. 1C), there has been speculation that this tissue might play a role in egg chamber elongation (Delon and Brown, 2009; Horne-Badovinac, 2014). We will provide evidence that the muscle sheath does contribute to this morphogenesis, but that it does so by promoting germ cell growth.

Here we show that depletion of Laminin from muscle sheath BM causes a progressive, dystrophic phenotype in this tissue. We then use the resulting changes in muscle sheath contractility to probe this tissue's function in egg chamber elongation. During late stages of

Development (2016) 143, 1375-1387 doi:10.1242/dev.131276

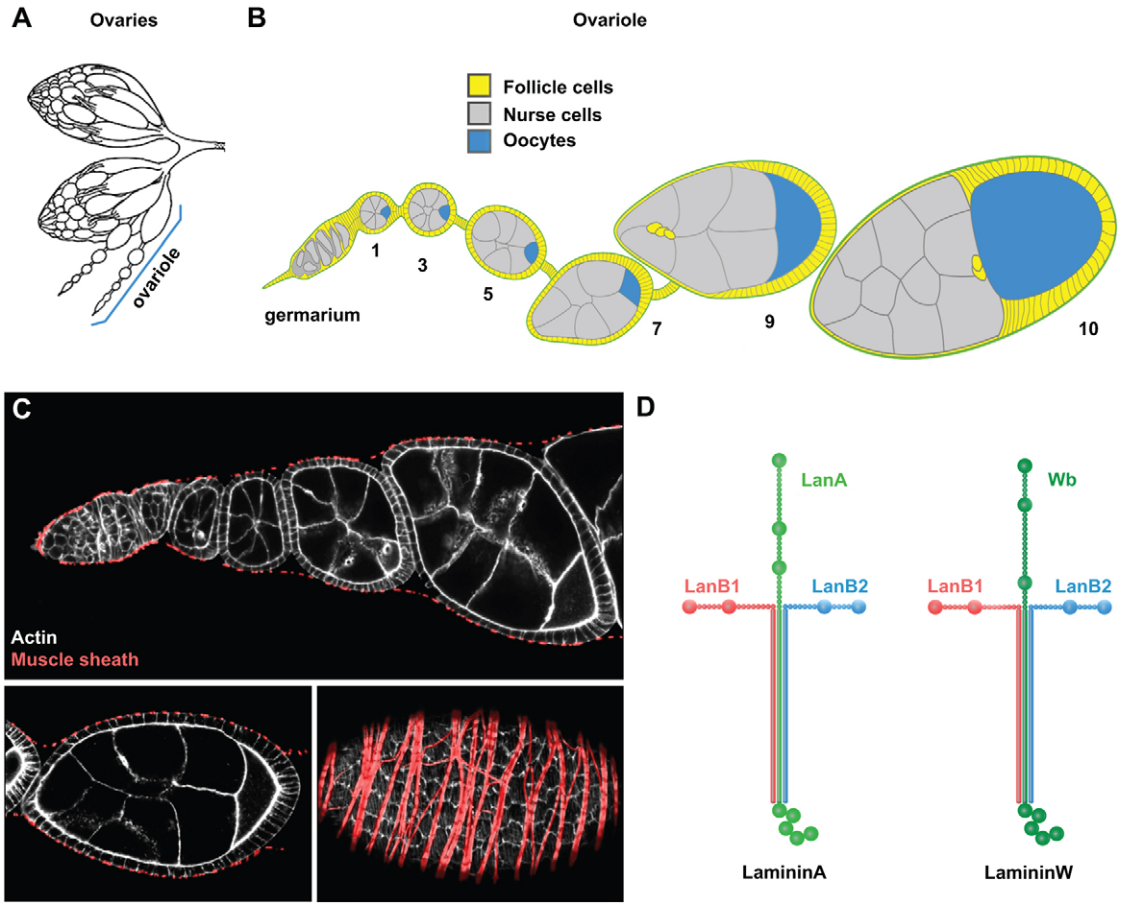

Fig. 1. Introduction to *Drosophila* ovary structure and Laminin isoforms. (A) A pair of ovaries with two ovarioles highlighted. Modified from Miller (1950), used with permission from Cold Spring Harbor Laboratory Press. (B) An ovariole showing egg chamber morphology at several stages. Ovarian muscles are not shown. (C) Micrographs showing how the muscle sheath envelops the egg chambers. All cells are stained with Phalloidin. The muscle sheath has been false colored red. Ovariole (top panel), transverse (bottom left) and surface views of the same egg chamber (bottom right). (D) Schematic of *Drosophila*'s two Laminin isoforms, LamininA and LamininW.

degeneration, the muscle sheath is hypo-contractile. This condition leads to a defect in yolk uptake by the oocyte and a shortening of the egg. These observations reveal a previously unappreciated role for the muscle sheath in egg chamber development and demonstrate the necessity of germ cell growth for its elongation. By contrast, during early stages of degeneration, the muscle sheath is hyper-contractile. This condition correlates with both precocious and enhanced elongation in the egg chamber, likely through direct circumferential compression. Although the muscle sheath does not compress the egg chambers in this way under normal conditions, this observation suggests that the mechanical environment that the egg chamber experiences can contribute to final egg shape. Together, this work highlights how physical contributions from multiple tissues can be integrated to shape an organ.

RESULTS

Laminin and Dystroglycan are required in the muscle sheath for proper egg shape

Laminin is a heterotrimeric protein that is an essential component of BMs. *Drosophila* has two Laminin isoforms: LamininA and LamininW (Fig. 1D). These proteins share a β-chain (LanB1) and a γ-chain (LanB2), but differ in their α-chains. LamininA's α-chain is LanA, whereas LamininW's is Wing blister (Wb). Loss of LanA from the follicular BM disrupts egg chamber elongation (Frydman and Spradling, 2001), producing eggs with a reduced aspect ratio (length/width) (Fig. 2A). By contrast, Wb is not thought to be expressed in the follicle cells, except the border cells (Schneider et al., 2006). Thus, Wb's function in egg chamber elongation is unexplored.

To investigate whether Wb contributes to egg chamber elongation, we analyzed two *wb-RNAi* transgenes: TRIP.JF03238 (*wb-RNAi-a*) and v108020 (*wb-RNAi-b*). These transgenes target different regions of the *wb* transcript, and both induce blisters in adult wings (Fig. S1B). Moreover, these and all other RNAi transgenes in this paper have been used in previous studies (Table S1). We expressed the *wb-RNAi* transgenes in the somatic tissues of the ovary using *traffic jam-Gal4* (*tj-Gal4*) (Fig. 2B,B′). Intriguingly, both reduced the egg's aspect ratio (Fig. 2C). Thus, even though Wb is likely not expressed in the follicle cells, it is still required for proper egg shape.

Although *tj-Gal4* is commonly used for transgene expression in the follicular epithelium, this driver also expresses in the muscle sheath (Fig. 2B,B′, arrowhead). Given that the muscle sheath has two BMs, one on either side of the cellular layer (Cummings, 1974), depletion of Wb from this tissue might cause the egg shape defect. *Mef2-Gal4* is expressed in the muscle sheath, but not the follicle cells (Fig. 2D,D′) (Hudson et al., 2008). Expressing *wb-RNAi-a* with this driver decreases the egg's aspect ratio (Fig. 2E), similar to *tj-Gal4*. Although using *Mef2-Gal4* to drive *wb-RNAi-b* is lethal for unknown reasons, when expression is restricted to adult stages with a temperature-sensitive version of the Gal4 antagonist Gal80

Development (2016) 143, 1375-1387 doi:10.1242/dev.131276

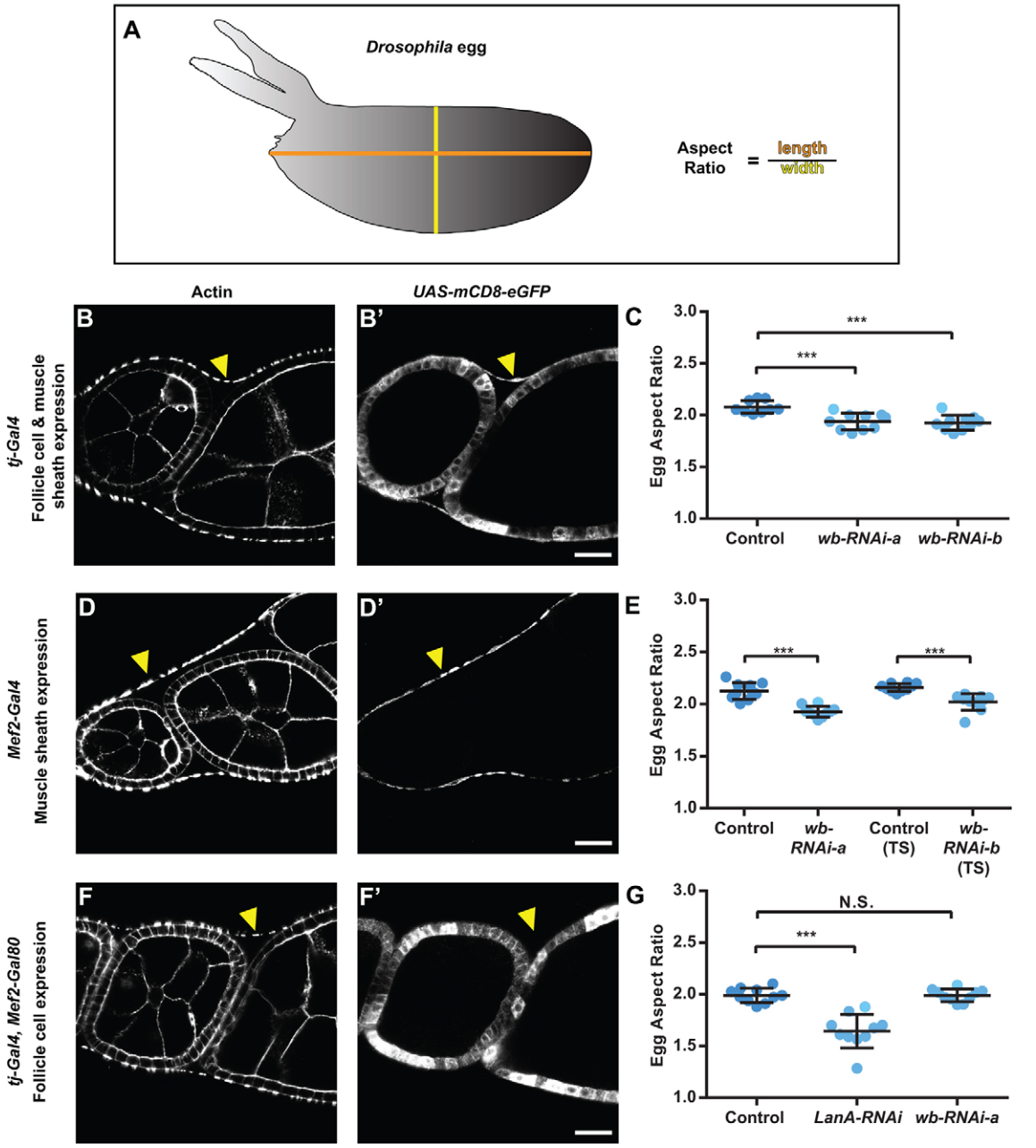

Fig. 2. Wb is required in the muscle sheath to shape the egg. (A) Schematic showing how egg aspect ratio was measured. (B) *tj-Gal4* drives *UAS-mCD8-eGFP* in the follicle cells and muscle sheath (arrowheads). (C) *tj-Gal4* driving *wb-RNAi* decreases the egg's aspect ratio. (D) *Mef2-Gal4* drives *UAS-mCD8-eGFP* in the muscle sheath (arrowheads), not the follicle cells. (E) *Mef2-Gal4* driving *wb-RNAi* also decreases the egg's aspect ratio. (F) *tj-Gal4, Mef2-Gal80* drives *UAS-mCD8-eGFP* in the follicle cells, but not the muscle sheath (arrowheads). (G) *tj-Gal4, Mef2-Gal80* driving *LanA-RNAi* decreases the egg's aspect ratio. Driving *wb-RNAi* has no effect. Scale bars: 20 µm. Data represent mean±s.d., Student's *t*-test; N.S., not significant; ***P<0.001; n=9-10 eggs per condition. Newly eclosed females were cultured for 6 days at 29°C.

(McGuire et al., 2004), this transgene also decreases egg aspect ratio (Fig. 2E). This same phenotype is observed when *Mef2-Gal4* is used to deplete LanA, LanB1 or the Laminin receptor Dystroglycan (Dg) from the muscle sheath by RNAi (Fig. S1C). Moreover, we have confirmed that Laminin is produced by muscle cells by showing that *Mef2>wb-RNAi-a* and *Mef2>LanB1-RNAi* both reduce Laminin levels in the muscle sheath BMs (Fig. S2). Thus, both Laminin isoforms and Dystroglycan all appear to be required in the muscle sheath for proper egg shape.

To confirm that Wb does not function in the follicle cells to shape the egg, we combined *tj-Gal4* with the *Mef2* regulatory regions expressing Gal80 (*tj-Gal4, Mef2-Gal80*), which drives transgene expression in the follicle cells, but not the muscle sheath (Fig. 2F,F′). As a positive control, we used *tj-Gal4, Mef2-Gal80* to deplete LanA from the follicle cells by RNAi. This condition mimics a *LanA* mutation by reducing the egg's aspect ratio (Fig. 2G) (Frydman and Spradling, 2001). By contrast, depleting solely Wb from the follicle cells has no effect (Fig. 2G). Together, these data suggest that whereas LanA acts in the follicle cells and muscle sheath to shape the egg, Wb is only required in the muscle sheath; however, analysis of a *wb* null allele will be required to validate this assertion.

Development (2016) 143, 1375-1387 doi:10.1242/dev.131276

Wb depletion causes a dystrophic phenotype that reduces muscle sheath contractility

Several human muscular dystrophies are caused by mutations in Laminin or components of the Dystrophin glycoprotein complex (DGC), which includes Dystroglycan (Wallace and McNally, 2009). These proteins protect muscle plasma membranes from contraction-induced damage by providing a linkage between the BM and actin cytoskeleton (Ervasti and Sonnemann, 2008; Holmberg and Durbeej, 2013; Ozawa et al., 2001). When this linkage is disrupted, micro-tears form within the plasma membranes that allow extracellular fluids to enter the cell. Defects in Laminin or the DGC also result in a progressive loss of contractile function (Wallace and McNally, 2009). We therefore hypothesized that Wb depletion causes a dystrophic phenotype in the muscle sheath, and that the resulting reduction in muscle sheath contractility alters egg shape. To test this hypothesis, we first examined muscle sheath structure and function upon Wb depletion. For these experiments, females with *Mef2-Gal4* driving *wb-RNAi-a* were collected within 24 h of eclosion, and then cultured at 29°C for six days before their ovaries were dissected for analysis. We will refer to this condition as *Mef2>wb-RNAi(6d)*.

To determine whether Wb depletion damages muscle sheath plasma membranes, we incubated freshly dissected ovaries in the membrane-impermeable dye SYTOX Green, which only fluoresces when bound to DNA. Because muscle sheath cells are mononucleate (Hudson et al., 2008), each SYTOX-labeled nucleus represents one cell whose plasma membrane is breached. Whereas only 17% of nuclei are labeled under control conditions, this number jumps to 73% under *Mef2>wb-RNAi(6d)* (Fig. S3A,B). Notably, we also see large tears in some muscle fibers under this condition (Fig. S3E-G), which likely accounts for some labeled nuclei. These severely damaged fibers might be dying by necrosis, another phenotype common to dystrophic muscles (Wallace and McNally, 2009). Together, these data show that Wb depletion causes defects in muscle sheath integrity.

We next investigated how Wb depletion affects muscle sheath contractility. The sarcomere is the basic contractile unit in muscle (Fig. 3A). It is composed of thick filaments of myosin (the A-band)

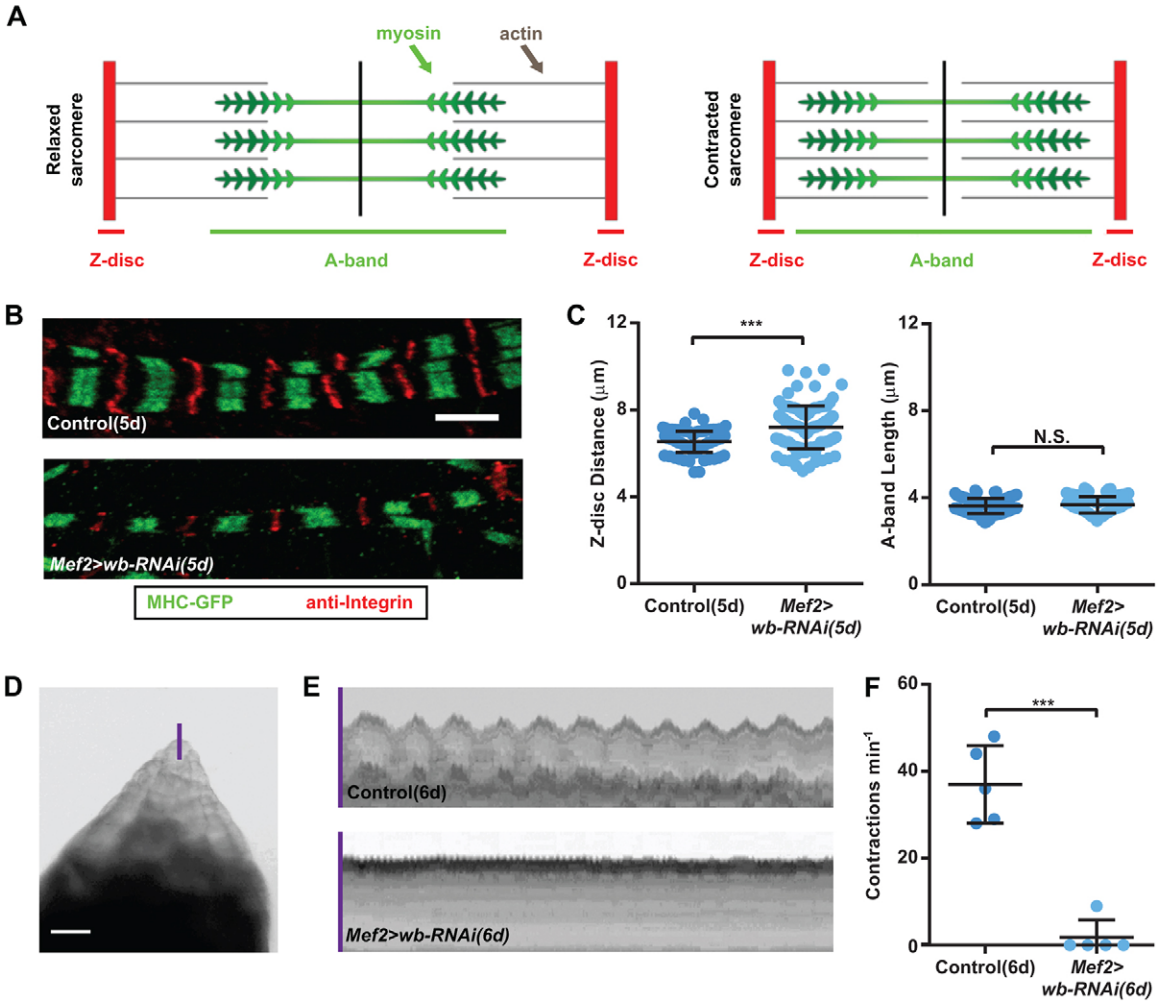

Fig. 3. Wb depletion largely eliminates muscle sheath contractions. (A) The sliding filament model for muscle contraction. (B,C) Effects of *Mef2>wb-RNAi(5d)* on sarcomere length. (B) Representative images of sarcomere structure in the muscle sheath overlying stage 10 egg chambers. A-bands (green) are marked with myosin heavy chain GFP (MHC-GFP) and Z-discs (red) are marked with an anti-integrin-βPS. (C) Average Z-disc distance is increased under *Mef2>wb-RNAi(5d)*, whereas A-band length is unchanged. *n*=100 sarcomeres per condition. (D-F) *Mef2>wb-RNAi(6d)* dampens ovarian contractions. (D) Movie still of an ovary in culture. The purple line corresponds to the control kymograph in E. (E) Representative kymographs showing ovarian contraction frequency. Contractions are largely eliminated under *Mef2>wb-RNAi(6d)*. (F) Quantification of the data in E. Data represent mean±s.d., Student's *t*-test; N.S., not significant; ***P<0.001. Scale bar: 5 µm in B, 100 µm in D.

Development (2016) 143, 1375-1387 doi:10.1242/dev.131276

and thin filaments of actin. The thin filaments are attached to Z-discs at the sarcomere boundaries. During contraction, myosin pulls on the actin, shortening the distance between the Z-discs. Under *Mef2>wb-RNAi(6d)*, where muscle fibers tear, the sarcomeres also become disorganized (Fig. S3E-G). Thus, we examined sarcomere structure in females cultured for five days at 29°C [*Mef2>wb-RNAi(5d)*]. Here, sarcomere structure was preserved, but the average distance between the Z-discs was increased, whereas A-band length was unchanged (Fig. 3B,C). This organization suggests that the muscle sheath is hypo-contractile even before the fibers tear.

Finally, we used live imaging to examine the effects of Wb depletion on muscle sheath function. When an ovary is placed in culture, it continues to rhythmically contract (Irizarry and Stathopoulos, 2015; Middleton et al., 2006). These whole-organ contractions are most prominent near the ovary's tip, and represent a composite of the contractions produced by muscle sheaths surrounding the ovarioles and the peritoneal sheath surrounding the ovary. Because *Mef2-Gal4* is expressed in both muscle types (Hudson et al., 2008), it is likely that both are affected by Wb depletion. Kymographs of these whole-ovary contractions reveal that this motion largely ceases in *Mef2>wb-RNAi(6d)* ovaries (Fig. 3D-F; Movie 1). Thus, the changes in muscle sheath structure seen under Wb depletion correlate with changes in contractile activity.

The muscle sheath lengthens the egg by promoting yolk uptake and oocyte growth

The data above suggest that Wb depletion causes a progressive, dystrophic phenotype in the muscle sheath that dampens its contractile activity. How does this reduce the egg's aspect ratio? According to the molecular corset model, a defect in egg chamber elongation could be caused by disruption of the molecular corset in the follicular epithelium or by a reduction in germ cell growth. Manipulations that disrupt the molecular corset lower the egg's aspect ratio by both reducing its length and increasing its width, but do not change the egg's volume (Frydman and Spradling, 2001). By contrast, depleting Wb from the muscle sheath reduces egg length, while leaving the width intact (Fig. 4A-C). This observation indicates that egg volume is reduced and that a loss of muscle sheath contraction might indirectly affect germ cell growth. We have also confirmed that the molecular corset and egg chamber rotation are unperturbed in stage 7 egg chambers from *Mef2>wb-RNAi(6d)* females (Fig. S4A-C, Movie 2).

To determine how Wb depletion from the muscle sheath affects germ cell growth, we examined egg chambers at stage 10b, when the increase in germ cell volume is largely complete. In egg chambers from *Mef2>wb-RNAi(6d)* females, nurse cell volume is unaffected, but oocyte volume is reduced (Fig. 4D-F). These data suggest that

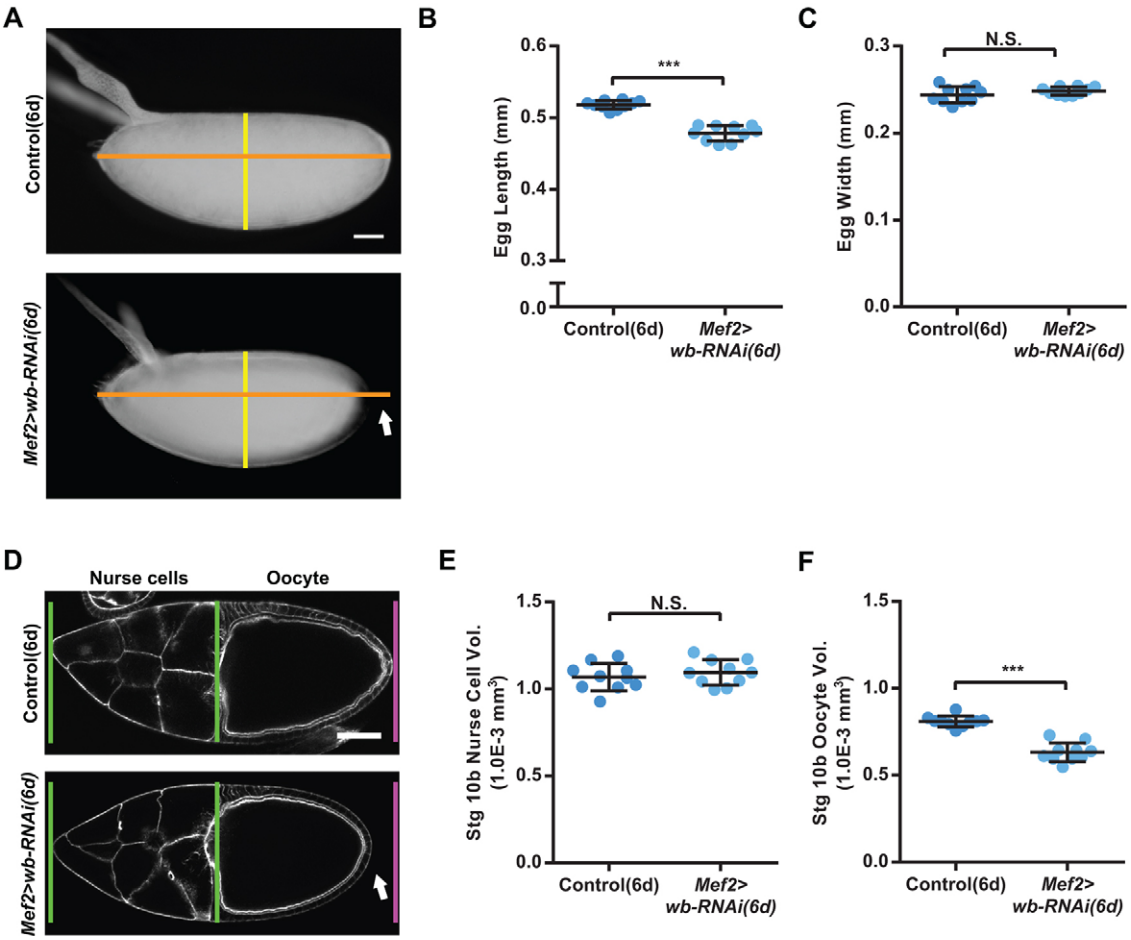

Fig. 4. Wb depletion reduces egg length and oocyte volume. (A) Representative images showing that egg length is reduced under *Mef2>wb-RNAi(6d)* (arrow), whereas the width is unchanged. Orange and yellow reference lines are the same length on both images. (B,C) Quantification of the data shown in A. (D) Representative images showing that oocyte size is reduced at stage 10b (arrow) under *Mef2>wb-RNAi(6d)*. Green and pink lines are the same distance apart on both images. (E,F) Measurements of germ cell volume at stage 10b. Under *Mef2>wb-RNAi(6d)*, nurse cell volume is normal (E), but oocyte volume is reduced (F). Data represent mean±s.d., Student's *t*-test; N.S., not significant; ***P<0.001; n=9-10 eggs/egg chambers per condition. Scale bars: 50 µm.

Development (2016) 143, 1375-1387 doi:10.1242/dev.131276

muscle sheath contraction promotes oocyte growth, likely through vitellogenesis.

To further investigate this idea, we examined the yolk proteins directly. There are three yolk proteins in *Drosophila*: Yp1, Yp2 and Yp3. Although some yolk proteins are produced by the follicle cells, the majority are synthesized in the fat body and secreted into the hemolymph (Bownes, 1982). These proteins reach the oocyte by passing in between the cells that make up the muscle sheath and follicular epithelium. Once endocytosed by the oocyte, yolk proteins are stored in autofluorescent granules. The density and fluorescence intensity of these granules are both reduced in stage 10b oocytes from *Mef2>wb-RNAi(6d)* females (Fig. 5A,B). Yolk proteins also accumulate to abnormal levels in the hemolymph of these females (Fig. 5C), a phenotype observed

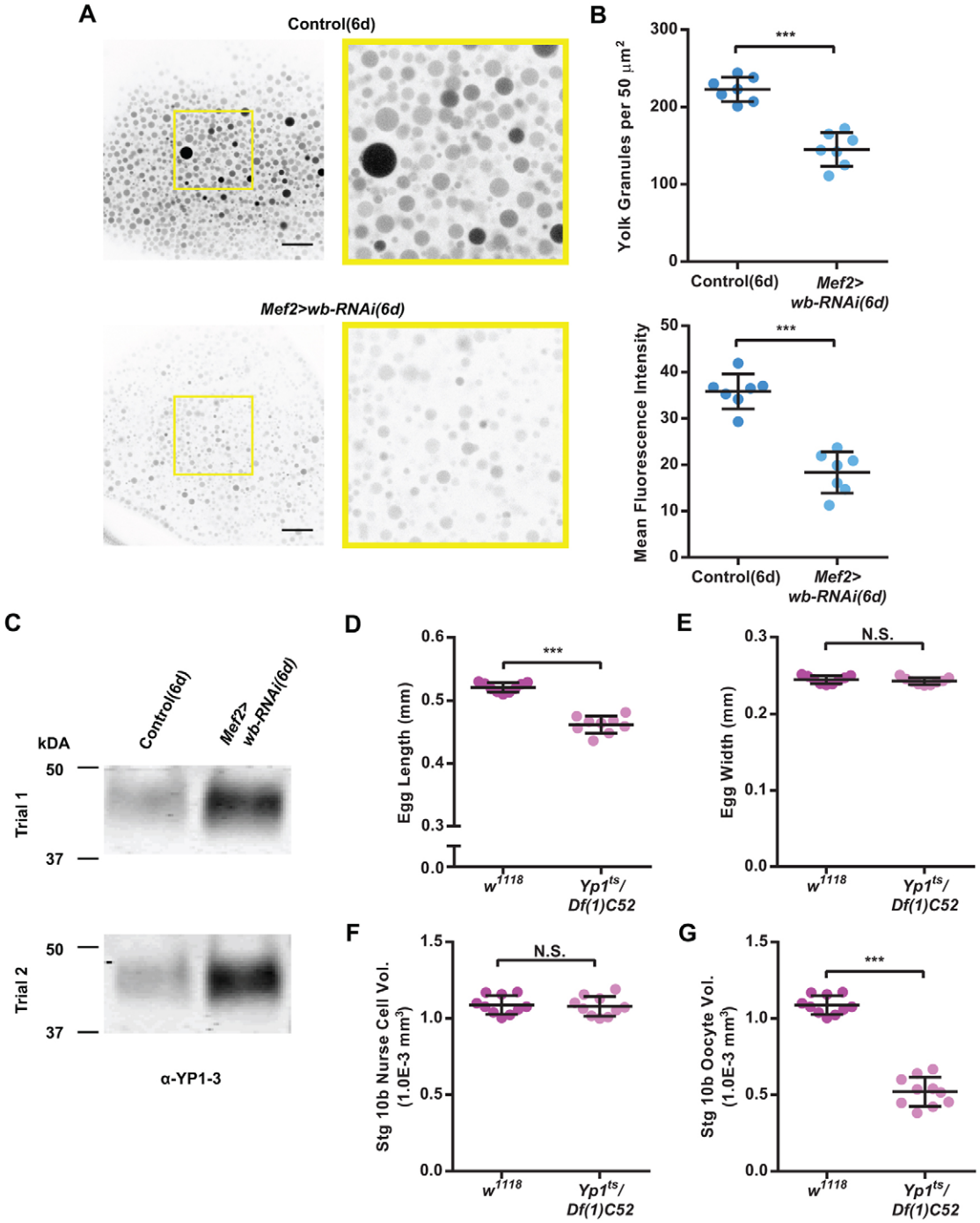

Fig. 5. Wb depletion reveals a role for the muscle sheath in vitellogenesis. (A) Representative images showing that the density and mean autofluorescence of yolk granules is reduced under *Mef2>wb-RNAi(6d)* at stage10b. The yellow boxes on the images on the left indicate regions shown in higher magnification on the right. Scale bars: 20 µm. (B) Graphs quantifying the effect shown in A. *n*=7 egg chambers per condition. (C) Western blot showing that yolk protein levels are increased in the hemolymph under *Mef2>wb-RNAi(6d)*. Two independent experiments are shown. Please see Materials and Methods for a discussion of loading controls. (D-G) Measurements performed on egg chambers from females where yolk protein levels have been reduced genetically ($Yp1^{ts}$/*Df(1)C52*). This condition has a similar effect to *Mef2>wb-RNAi(6d)*, as egg length (D,E) and stage 10b oocyte volume (F,G) are both selectively reduced. Data represent mean±s.d., Student's *t*-test; N.S., not significant; ***P<0.001; *n*=9-10 eggs/egg chambers per condition in D-G.

Development (2016) 143, 1375-1387 doi:10.1242/dev.131276

in other conditions that impair yolk uptake (DiMario and Mahowald, 1987). Finally, we asked whether a vitellogenesis defect is sufficient to reduce the egg's length and volume by lowering yolk protein levels genetically (*Yp1*^{ts}*/Df(1)C52*, see Materials and Methods). Similar to *Mef2>wb-RNAi(6d)*, egg length and stage 10b oocyte volume are both selectively reduced in these flies (Fig. 5D-G).

Because *Mef2-Gal4* is expressed in most (if not all) muscles (Ranganayakulu et al., 1998, 1995), we needed to show that perturbing muscle sheath function by a different method changed the egg's shape in the same way. When germaria are dissected from the ovary of one female and injected into the abdomen of another, strings of egg chambers can be produced that develop in the absence of a muscle sheath (Fig. 6A) (Lin and Spradling, 1993; Srdic and Jacobs-Lorena, 1978). We found that eggs produced by this method are similar to those that develop either inside a hypo-contractile muscle sheath or with reduced yolk protein levels – their average length is reduced, but average width is unaffected (Fig. 6B,C). These values are more variable, however. Stage 10b oocyte volume is also selectively reduced under these conditions (Fig. 6D,E). Together, these data suggest a model wherein ovarian muscles stimulate vitellogenesis, which then helps to lengthen the egg.

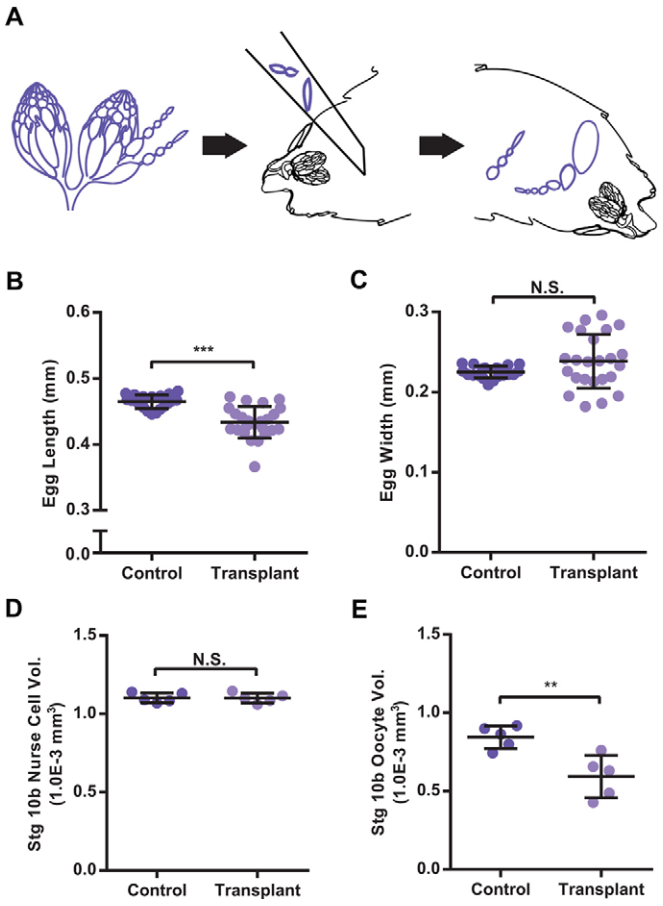

Fig. 6. Eggs that develop outside the muscle sheath have reduced length. (A) Schematic for germarium transplantation. Modified from Miller (1950), used with permission from Cold Spring Harbor Laboratory Press. (B,C) Eggs that develop outside the muscle sheath have reduced length (B) and normal width (C); *n*=20-24 eggs per condition. (D,E) At stage 10b, nurse cell volume is normal (D) and oocyte volume is reduced (E); *n*=5 egg chambers per condition. Data represent mean±s.d., Student's *t*-test; N.S., not significant; ***P*<0.01, ****P*<0.001.

Nurse cell dumping also contributes to egg length

To explore the relationship between oocyte growth and egg chamber elongation more fully, we also examined two conditions that reduce oocyte volume in a different way. After vitellogenesis is complete, the nurse cells transfer their cytoplasm to the oocyte in a process called nurse cell dumping (Robinson and Cooley, 1997). Strong dumping defects cause oogenesis to fail. However, weak defects can produce relatively normal eggs with reduced volume. Conditions producing these weak defects include a viable missense mutation in *singed* (*sn*^{G409E}) (Cant and Cooley, 1996), which encodes an F-actin bundling protein also known as Fascin, and mutations in *bullwinkle* (*bwk*) (Rittenhouse and Berg, 1995), which encodes a putative transcription factor. In both cases, we find that egg length is selectively reduced, whereas its width is normal (Fig. 7A-C). These data provide yet more evidence that oocyte growth helps to lengthen the egg.

Wb depletion can induce a hyper-contractile state in the muscle sheath

Mef2>wb-RNAi(6d) consistently produces eggs with a reduced aspect ratio; however, during our early work with *Mef2-Gal4*, we noticed that the average aspect ratio of the egg varied with the time that females were cultured after eclosion. To better document this phenomenon, we performed a time course experiment. Newly eclosed females with *Mef2-Gal4* driving *wb-RNAi-a* were placed at 29°C and then collected for dissection and egg aspect ratio measurements on a daily basis for seven days. Interestingly, eggs collected on the first day have an aspect ratio that is increased compared with controls. This value then decreases over time until it reaches its minimum at day six (Fig. 8A). Depletion of Dystroglycan shows a similar trend (Fig. 8B).

Muscular dystrophy is a progressive condition wherein the initial mutagenic insult often causes only moderate tissue damage; the damage then worsens over time as the muscle is used (Wallace and McNally, 2009). Interestingly, some dystrophic muscles show hyper-contractility during early stages of their degeneration (Cullen and Fulthorpe, 1975; Gupta et al., 2012; Haines et al., 2007). We hypothesized, therefore, that the eggs with an increased aspect ratio might have developed within a hyper-contractile muscle sheath. To investigate this possibility, we examined muscle sheath structure and function in females with *Mef2-Gal4* driving *wb-RNAi-a* that were collected within 24 h of eclosion, then cultured for one day at 29°C before their ovaries were dissected [*Mef2>wb-RNAi(1d)*].

Similar to the hypo-contractile *Mef2>wb-RNAi(6d)* condition, the muscle sheaths from *Mef2>wb-RNAi(1d)* females have defects in plasma membrane integrity, as shown by SYTOX Green (Fig. S3C,D). Unlike the *Mef2>wb-RNAi(6d)* condition, however, the average distance between the sarcomeric Z-discs in *Mef2>wb-RNAi(1d)* females is reduced compared with controls (Fig. 8C,D). Moreover, the frequency of whole-ovary contractions is increased, although their amplitude is reduced (Fig. 8E-G; Movie 3). These data show that the muscle sheath is hyper-contractile during the early stages of degeneration.

A hyper-contractile muscle sheath augments egg chamber elongation

We next used *Mef2>wb-RNAi(1d)* to explore how muscle sheath hyper-contraction increases egg aspect ratio. Interestingly, this condition reduces the egg's width while leaving its length unchanged (Fig. 9A-C). Because only one dimension is affected, this condition also reduces the egg's volume. Consistent with this observation, oocyte volume is selectively reduced at stage 10b in

Development (2016) 143, 1375-1387 doi:10.1242/dev.131276

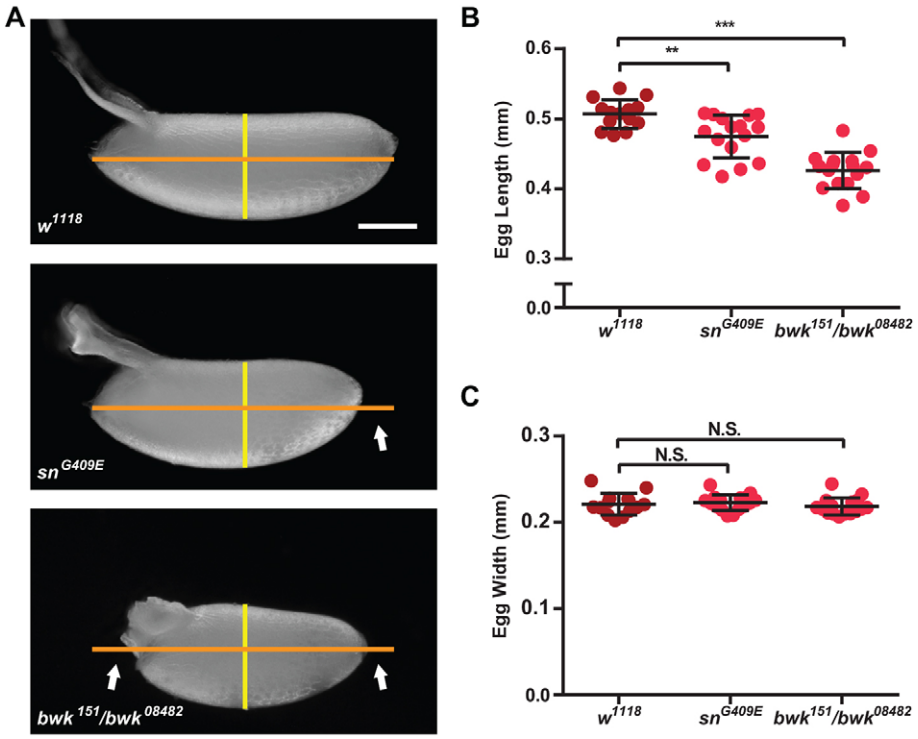

Fig. 7. Weak defects in nurse cell dumping reduce egg length. (A) Representative images showing that egg length is reduced under two conditions that cause weak nurse cell dumping defects (arrows), whereas the width is unchanged. (B,C) Quantification of the data shown in A. Data represent mean±s.d., Student's *t*-test; N.S., not significant; $^{**}P<0.01$, $^{***}P<0.001$; n=14-16 eggs per condition. Scale bars=50 µm.

Mef2>wb-RNAi(1d) females (Fig. 9D,E), which suggests that an increased rate and/or reduced amplitude of muscle sheath contraction also perturbs vitellogenesis. The reduction in oocyte volume and yolk granule density in *Mef2>wb-RNAi(1d)* females is less than that seen under *Mef2>wb-RNAi(6d)*; however, the strength of the vitellogenesis defect increases over time as muscle degeneration worsens (Fig. S4G-J).

We have just shown, however, that impaired vitellogenesis reduces the egg's aspect ratio. Why then is the aspect ratio of these eggs increased? The molecular corset appears to be unaffected in stage 7 egg chambers from *Mef2>wb-RNAi(1d)* females (Fig. S4D-F, Movie 4). Instead, *Mef2>wb-RNAi(1d)* changes the way the muscle sheath envelops the egg chambers. Carefully dissected ovarioles can be binned into three classes based on muscle sheath morphology (Fig. 9F). In class 1 (tight), there are no spaces between the muscle sheath and egg chambers. In class 2 (normal), there are small spaces between the muscle sheath and egg chambers at the interface between adjacent egg chambers. In class 3 (loose), the muscle sheath appears dilated, younger egg chambers become bunched up on one another, and the spaces between the muscle sheath and egg chambers are irregular in size and frequency. Under control conditions, most ovarioles fall into class 2 (normal) (Fig. 9G,H). By contrast, under *Mef2>wb-RNAi(6)* (hypo-contractile) conditions, most ovarioles fall into class 3 (loose) (Fig. 9G), and under *Mef2>wb-RNAi(1d)* (hyper-contractile) conditions, most ovarioles fall into class 1 (tight) (Fig. 9H). These data suggest that the muscle sheath's contractility affects how it surrounds the egg chambers.

Given that the hyper-contractile *Mef2>wb-RNAi(1d)* muscle sheath tightly envelops developing egg chambers (Fig. 9F,H) and that individual muscle fibers are largely oriented perpendicular to the egg chamber's AP axis (Fig. 1C), we hypothesized that, under this aberrant condition, the muscle might exert a circumferential compressive force on the egg chambers that augments the molecular corset. In support of this notion, aspect ratios of egg chambers that develop within a *Mef2>wb-RNAi(6d)* hypo-contractile muscle sheath do not deviate from controls until stage 9, after vitellogenesis begins (Fig. 9I). By contrast, egg chambers that develop within a *Mef2>wb-RNAi(1d)* hyper-contractile muscle sheath have increased aspect ratios across all stages examined (4-14) (Fig. 9J). The observation that egg chambers are elongated at stage four is particularly intriguing, as wild-type egg chambers have not yet begun to elongate at this stage. Thus, muscle sheath hyper-contractility correlates with both precocious and enhanced elongation of the egg chamber.

DISCUSSION

Here we have shown that Wb depletion causes a phenotype in ovarian muscle sheaths that shares many similarities with human muscular dystrophies. Specifically, Wb depletion appears to initiate a damage cascade that is characterized by defects in plasma membrane integrity and hypercontraction at early stages of the degeneration process, followed by loss of contractile activity and gross defects in muscle integrity at later stages of degeneration. *Drosophila* has been a useful model for the study of muscular dystrophy, as mutations in homologs of several human disease genes also cause dystrophic phenotypes in flies (Plantié et al., 2015). For example, mutations in *dystrophin* (Duchenne muscular dystrophy), *sarcoglycan gamma* and/or *delta* (limb girdle muscular dystrophy), *protein O-mannosyltransferase 1/2* (Walker–Wardburg Syndrome), and *lamin A/C* (Emery–Dreifuss muscular dystrophy) all show this property (Allikian et al., 2007; Dialynas et al., 2010; Haines et al., 2007; Shcherbata et al., 2007). Wb is the homolog of human laminin subunit alpha 2 (Martin et al., 1999). Mutations in this gene cause one of the most prevalent muscular dystrophies, congenital muscular dystrophy type 1A. Our fortuitous discovery that Wb depletion causes a dystrophic phenotype in ovarian muscles now expands the repertoire of muscular dystrophies for which *Drosophila* genetics could be employed to dissect disease etiology and/or identify new therapies.

Development (2016) 143, 1375-1387 doi:10.1242/dev.131276

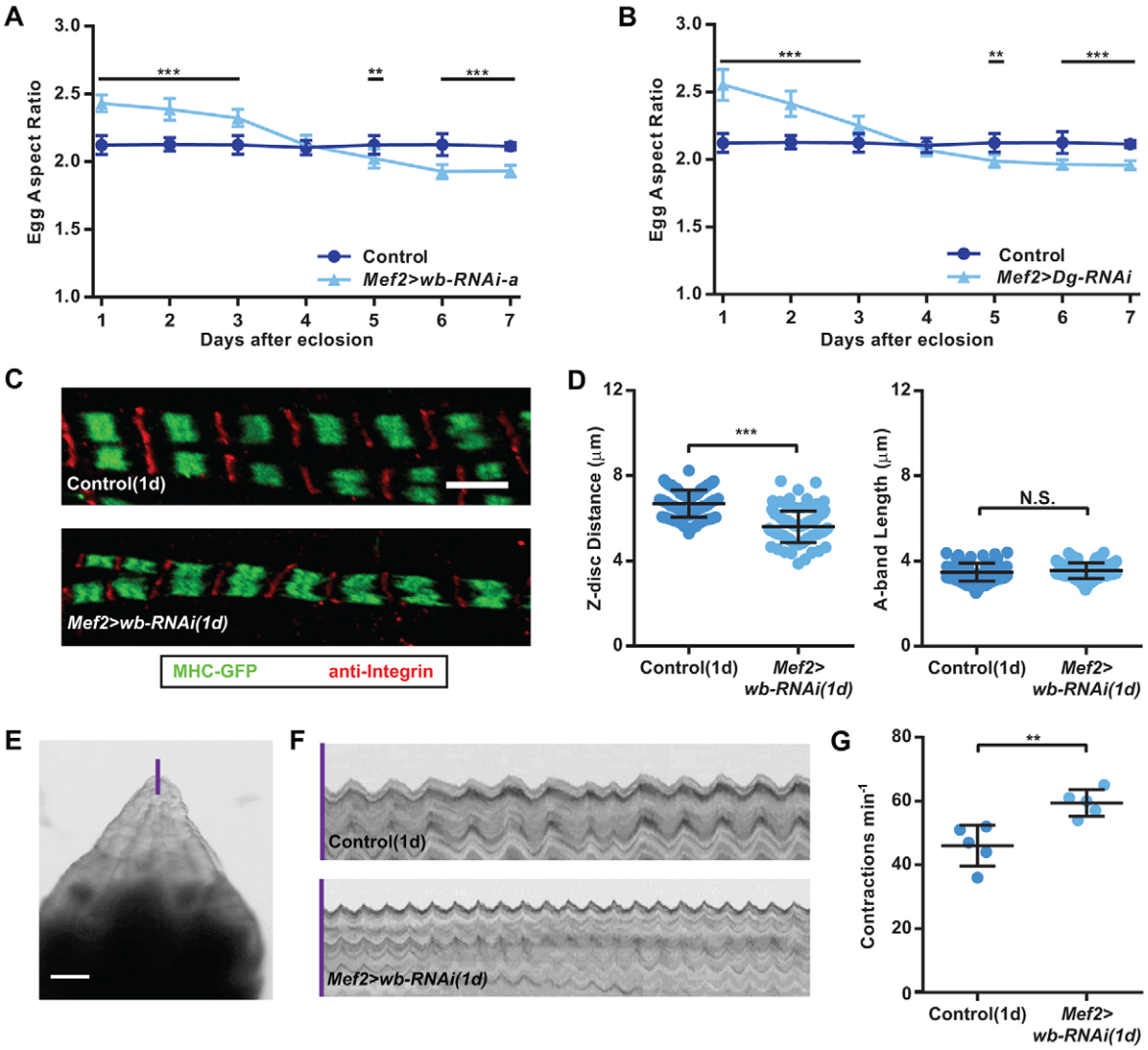

Fig. 8. Wb depletion can also cause muscle sheath hyper-contraction. (A,B) Depletion of either Wb or Dg from the muscle sheath can both increase and decrease the aspect ratio of the egg. Wb (A) and Dg (B) were depleted from the muscle sheath and egg aspect ratio was measured on a daily basis for one to seven days. Aspect ratio is initially increased, but decreases over time until it is below that of controls. *n*=9-10 eggs per genotype per day. (C,D) Effects of *Mef2>wb-RNAi(1d)* on sarcomere length in the muscle sheath overlying stage 10 egg chambers. (C) Representative images where A-bands (green) are marked with myosin heavy chain GFP (MHC-GFP) and Z-discs (red) with anti-integrin-βPS. (D) The average Z-disc distance is decreased under *Mef2>wb-RNAi(1d)*, whereas A-band length is unchanged. *n*=100 sarcomeres per condition. (E-G) Effects of *Mef2>wb-RNAi(1d)* on ovarian contractions. (E) Movie still of an ovary in culture. The purple line corresponds to the control kymograph in F. (F) Representative kymographs showing ovarian contraction frequency is increased under *Mef2>wb-RNAi(1d)*. (G) Quantification of the data in F. Data represent mean±s.d., Student's *t*-test; N.S., not significant; ***P*<0.01, ****P*<0.001. Scale bar: 5 μm in C, 100 μm in E.

We have also used the changes in contractility seen upon Wb depletion to investigate this tissue's function in egg chamber development. Through this work, we discovered a role for ovarian muscles in vitellogenesis. Yolk proteins produced by the follicle cells are secreted from the apical epithelial surface and rapidly endocytosed by the oocyte (Trougakos et al., 2001). By contrast, yolk proteins secreted by the fat body into the hemolymph must penetrate deep into the ovary to reach developing oocytes. It is known that the dorsal vessel (insect heart) is insufficient to provide hemolymph circulation for all body regions (Pass, 2000). For example, 'wing hearts' are accessory pulsatile organs that specifically direct hemolymph into the wings (Tögel et al., 2008). We and others speculate that the rhythmic contraction of ovarian muscles could provide a similar function in the female abdomen, stimulating the local hemolymph flows necessary for the yolk proteins to penetrate the ovary (Cook and Peterson, 1989; Cruickshank, 1973; Gutzeit and Haas-Assenbaum, 1991; Middleton et al., 2006). Early support for this model came from studies in the flour moth *Anagasta kühniella* (Cruickshank, 1973). When horseradish peroxidase (HRP) was added to cultured *Anagasta* ovaries, HRP accumulated between the follicle cells of vitellogenic egg chambers at a faster rate than predicted for diffusion. Performing the same experiment with muscle contractions dampened largely abrogated HRP movement into the ovary. We now provide the first *in vivo* evidence for this model by showing that reduced ovarian muscle contraction correlates both with increased yolk proteins in the hemolymph and decreased yolk granule density in oocytes. Moreover, the frequency and/or amplitude of muscle contractions appear to be important as *Mef2>wb-RNAi(1d)* also reduces oocyte volume, although to a lesser extent. Because our Wb depletion experiments likely affect both the muscle sheath and peritoneal sheath, we cannot distinguish

Development (2016) 143, 1375-1387 doi:10.1242/dev.131276

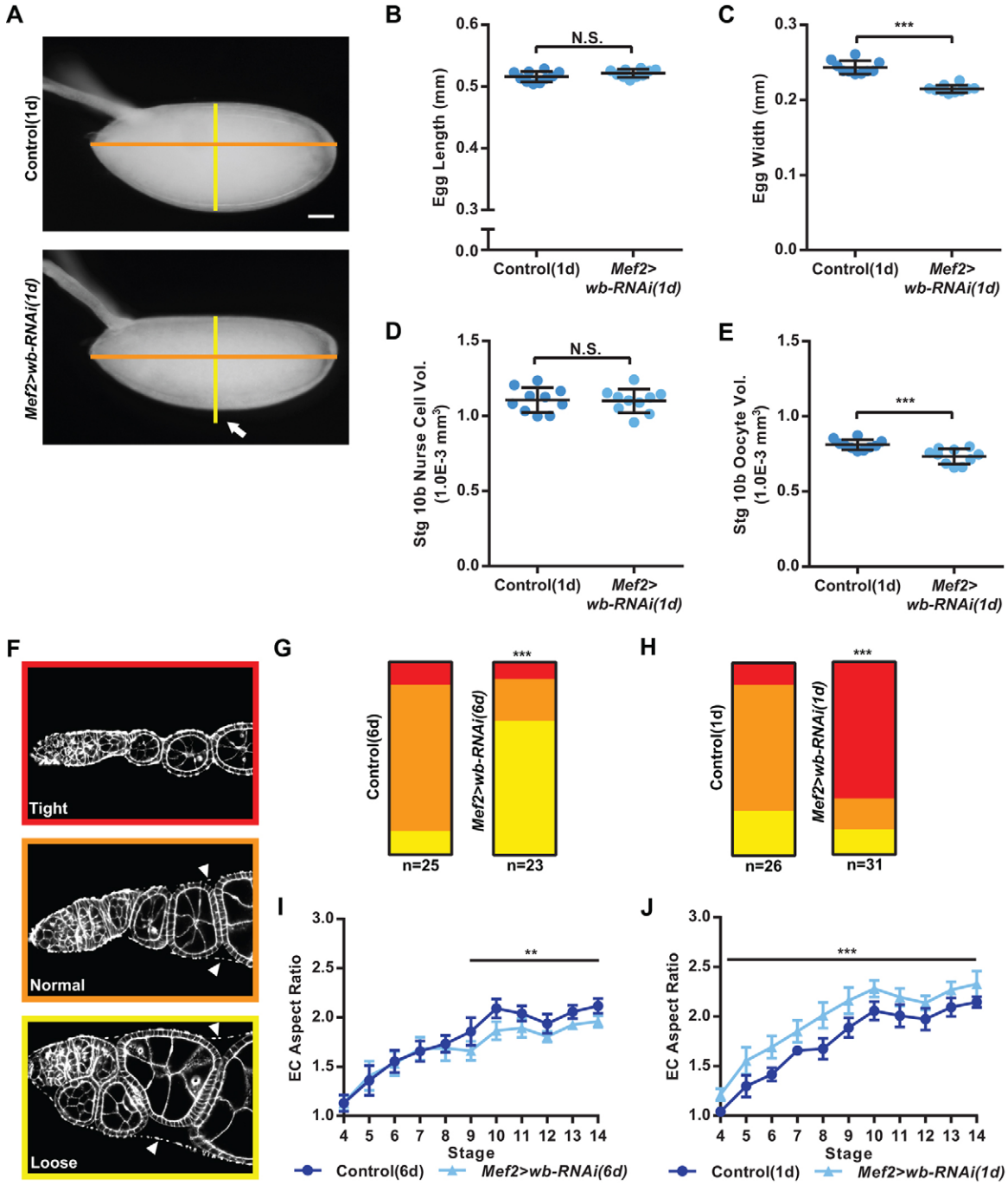

Fig. 9. A hyper-contractile muscle sheath enhances egg chamber elongation. (A) Representative images showing that egg width is reduced under *Mef2>wb-RNAi(1d)* (arrow), whereas length is unchanged. Orange and yellow reference lines are the same length on both images. Scale bar: 50 µm. (B,C) Quantification of egg length and width data in A. (D,E) Measurements of germ cell volume at stage 10b. Under *Mef2>wb-RNAi(1d)*, nurse cell volume is normal (D), but oocyte volume is reduced (E). (F-H) Wb depletion affects the way the muscle sheath envelops the egg chambers. (F) Muscle sheath morphology can be binned into three categories; tight, normal and loose. Arrowheads mark gaps between the muscle sheath and the egg chambers. (G,H) Quantification of muscle sheath morphology. (G) In controls, the normal morphology predominates. Under *Mef2>wb-RNAi(6d)*, the loose morphology predominates. (H) Under *Mef2>wb-RNAi(1d)*, the tight morphology predominates. (I,J) Aspect ratio measurements across stages 4-14. (I) The aspect ratio for *Mef2>wb-RNAi(6d)* egg chambers does not fall below controls until stage 9, after vitellogenesis begins. (J) By contrast, the aspect ratio for *Mef2>wb-RNAi(1d)* egg chambers is higher than controls from stage 4. Data represent mean±s.d., Student's *t*-test in B-E,I,J, Chi squared test in G,H; N.S., not significant; ***P*<0.01, ****P*<0.001; *n*=9-10 egg chambers per condition except where noted in G,H.

the relative contributions of these muscle types to vitellogenesis, but envision that both are involved.

Our ability to alter muscle sheath contractility has also elucidated the mechanisms controlling egg chamber elongation. According to the molecular corset model, pressure exerted by germ cell growth should play a central role in elongation. Our finding that mild defects in vitellogenesis and nurse cell dumping both reduce the egg's length but not its width provides the first direct evidence for this idea. Unlike some conditions that disrupt vitellogenesis (Butterworth et al., 1992; DiMario and Mahowald, 1987), the

Development (2016) 143, 1375-1387 doi:10.1242/dev.131276

eggs produced by Wb depletion have normal opercula and vitelline membranes, making it easy to detect the change in aspect ratio. Moreover, because ovarian contractions promote vitellogenesis, we have also identified a role for ovarian muscles in shaping the egg.

We have further shown that muscle hyper-contraction correlates both with precocious and enhanced elongation in the egg chamber. We speculate that this change in the morphogenetic program is a result of circumferential compression of the egg chambers by the muscle sheath; however, force measurements are required to confirm this assertion. Notably, the muscle sheath does not play such a role in egg chamber elongation under normal conditions, as average egg width does not change when egg chambers develop either within a hypo-contractile muscle sheath or outside the muscle sheath (Fig. 5E, Fig. 6C). However, the involvement of the muscle sheath in egg elongation under conditions of hyper-contraction might still provide important information about the role of tissue mechanics in this process. For the egg chamber to adopt a permanent elongated shape, there must be changes in both the shape and relative positions of the cells within the follicular epithelium (reviewed in Horne-Badovinac, 2014). Our data suggest that an exogenous circumferential compression applied to the epithelium might be sufficient to induce these changes. This observation thus lends plausibility to the idea that forces exerted on this epithelium by the interaction between germ cell expansion and an external corset structure could produce a similar result.

Our finding that changes in muscle sheath contractility can both reduce and enhance egg chamber elongation indicates that care must be taken when studying this process. We discovered both normal and acquired roles for the muscle sheath in egg chamber elongation by depleting Wb, a protein expressed in the muscle but not the follicle cells. However, there are likely to be many proteins required for egg chamber elongation that function in both tissues. One notable example is the DGC, which is required in the follicle cells for basal actin bundle alignment (Deng et al., 2003). By depleting Dystroglycan, we now know that the DGC is also required in the muscle sheath for normal contractility (Fig. 8B, and data not shown). If *Gal4* drivers expressed in both tissues are used to deplete DGC proteins by RNAi, or if known combinations of mutant alleles that produce viable adults are studied (Shcherbata et al., 2007), any resulting changes in egg chamber shape will likely be because of a combinatorial effect of losing the protein both from the follicle cells and the muscle sheath. This concern can be alleviated by using the *Mef2-Gal4* and *tj-Gal4, Mef2-Gal80* drivers to ensure that the protein is depleted solely from one tissue or the other, or by producing genetic mosaics where a given phenotype can be tied to the presence of a mutant clone (Duffy et al., 1998; Hudson et al., 2008).

In summary, this work demonstrates that, even in a relatively simple system like egg chamber elongation, there are at least three cell types – the follicle cells, germ cells and ovarian muscles – that all make distinct physical contributions to the elongation program. Thus, these findings shed light on the complex cellular inputs required for organ morphogenesis.

MATERIALS AND METHODS

Drosophila genetics

Experimental genotypes and transgene expression conditions are in Table S2. Most fly lines were obtained from the Bloomington Stock Center with the following exceptions: *UAS-LanB1-RNAi*^{v23121}, *UAS-wb-RNAi*^{v108020}, *UAS-Dg-RNAi*^{v107029} and LanB1-GFP (FlyFos collection) are from Vienna *Drosophila* Resource Center (Vienna, Austria); *vkg-GFP*^{CC00791} is from Buszczak et al. (2007); *traffic jam-Gal4* is from the *Drosophila* Genetic Resource Center (Kyoto, Japan); *sn*^{G409E} is from Lynn Cooley (Cant and Cooley, 1996); *bwk*^{08482} and *bwk*^{151} are from Celeste Berg (University of Washington, WA, USA) (Rittenhouse and Berg, 1995); *Mef2-Gal80* (*mb247-Gal80*; also known as *mbGal80*; http://flybase.org/reports/FBtp0053293.html; contains a 247-bp fragment of the *Mef2* promoter) is from Martin Heisenberg (Lehrstuhl für Genetik und Neurobiologie, Würzburg, Germany). For RNAi experiments, females were collected within 24 h of eclosion and aged on yeast with males; fresh yeast was provided every other day. To lower yolk protein levels, a temperature-sensitive allele of *Yp1* (*Yp1*^{ts}) (Bownes and Hames, 1978) was placed over a deficiency removing *Yp1* and *Yp2* [*Df(1)C52*], and newly eclosed females were cultured at 29°C for 1 d before dissection.

Aspect ratio measurements

Most aspect ratio measurements were performed on stage 14 egg chambers or mature eggs ('eggs') dissected from the ovaries of experimental females (unless otherwise noted). Those shown in Fig. 7 were performed on laid eggs with complete chorions.

Immunohistochemistry and microscopy

Ovaries were dissected in S2 medium and fixed for 15 min in PBS+0.1% Triton X-100 (PBT)+4% EM-grade formaldehyde (Polysciences). TRITC-Phalloidin (1:200, Sigma, P1951) or Alexa Fluor 647-Phalloidin (1:50, Invitrogen, A22287) marked actin. Antibody stains were performed in PBT and detected with Alexa Fluor 488- or 555-conjugated secondary antibodies (1:200; Invitrogen, A21206 or A31570). Samples were mounted in SlowFade Antifade (Invitrogen). Antibodies: rabbit anti-GFP (1:200, Invitrogen, A6455), mouse anti-integrin-βPS (1:200 concentrate, DSHB, CF.6G11-c). Fluorescent images were obtained using Zeiss LSM 510 or LSM 880 confocal microscopes. Bright field images were taken with a Leica FluoIII microscope with Canon rebel camera. Image processing and measurements were performed in ImageJ (NIH) and Photoshop (Adobe). Graphs were generated and statistical analyses performed in Prism (GraphPad).

Sarcomere measurements

Images were taken midway along the AP axis of five ovarioles for each condition, with two fibers per image chosen for measurement. Ten adjacent sarcomeres were measured from gray-scale intensity plots of anti-integrin-βPS (Z-discs) and myosin heavy chain (MHC)-GFP anti-GFP staining (A-bands), respectively. Z-disc length is the distance between adjacent peaks; A-band length is the width of the curve, as previously described (Haines et al., 2007).

Live imaging of whole-ovary contractions

Ovaries were dissected in warm S2 media, and oviducts were removed. Movies were obtained with a Leica FluoIII microscope and Canon rebel camera. Kymographs corresponding to 1 min were generated using ImageJ. Contractions were counted as troughs in the kymograph.

Volume measurements

Z-stacks (1 µm interval) were taken through entire Phalloidin-stained stage 10b egg chambers. The Measure Stack plugin for ImageJ (OptiNav, Inc.) was used to measure the volumes of nurse cell and oocyte compartments. A region of interest (ROI) was selected on the first and last slice where the compartment was visible. Measure Stack interpolates the ROI for the slices between these points and calculates each ROI's area and the object's volume.

Yolk granule measurements

Ovaries were fixed and stained with Phalloidin. Yolk granules were induced to autofluoresce by illumination with a 405 nm laser, and images were taken 3 µm in from the oocyte membrane with a Zeiss LSM510 confocal microscope. A 50 µm^2 region in the center of each image was isolated for analysis. Mean fluorescence intensity of this region was measured in ImageJ and individual yolk granules were counted by hand.

Yp western blot

Hemolymph collection is described in supplementary Materials and Methods. The final dilution of hemolymph in SDS-PAGE sample buffer was boiled for 5 min before loading 15 µl onto a 4-15% polyacrylamide gel

Development (2016) 143, 1375-1387 doi:10.1242/dev.131276

(Bio-Rad). In-gel westerns were performed per LI-COR's instructions. Antibodies included: rabbit anti-YP (1:1250; Hames and Bownes, 1978) and an IRDye secondary (1:5000, LI-COR, 926-68023). Gels were imaged with Odyssey software v2.1 (LI-COR).

Because proteins typically used as loading controls are not present in hemolymph, we used Coomassie staining to ensure equivalent loading between lanes. After electrophoresis, each gel was divided into two sections; lower molecular weight bands versus higher molecular weight bands. The section with lower weight bands was stained with anti-Yp, the other with Coomassie. For both westerns, the Coomassie stain confirmed equivalent loading (data not shown).

Germarium transplants

One-day-old donor (*vkg-GFP*) and host (ovo^{D1}) females were aged on yeast with males for 3 days at 25°C. Donor ovaries were dissected in live imaging media (Prasad et al., 2007). After removing the muscle sheath from an ovariole, the germarium was isolated with a micro-knife (Fine Science Tools) and transferred to a drop of live imaging media on a silicone-coated slide. Two to three germaria were injected into one host abdomen using a glass needle attached to a syringe. Host females recovered for 3 days on yeast in individual vials at 25°C. Egg chambers dissected from host females that express Vkg-GFP were fixed and stained with Phalloidin for analysis.

Statistical analysis

All data were obtained from at least two independent experiments, and several females were analyzed each time. All data were highly reproducible. No statistical method was used to predetermine sample size. The sample sizes for each experiment are shown as individual data points on the graph itself, with a few exceptions. A Student's *t*-test was used to determine whether data from two experimental conditions were significantly different. This test is appropriate, because all data obtained follow an approximately normal distribution. Differences between experimental and control conditions were large in all cases and the variability within a single experimental condition was typically low. The experiments were not randomized. Egg chambers damaged by the dissection process were excluded from analysis.

Methods for supplementary information

Details on measurements of BM protein levels in the muscle sheath (Fig. S2), measurement of egg chamber rotation rates (Movies 2,4) and SYTOX Green staining (Fig. S3) are provided in the supplementary Materials and Methods.

Acknowledgements

We thank Tony Mahowald for insightful discussions about vitellogenesis and Graydon Gonsalvez for advice on detecting yolk autofluorescence. Chip Ferguson and members of the Horne-Badovinac lab provided helpful comments on the manuscript, and Nick Badovinac and Nate Ellis provided illustrations. We are also grateful to Lynn Cooley, Celeste Berg, Mary Bownes and Martin Heisenberg for generously providing reagents.

Competing interests

The authors declare no competing or financial interests.

Author contributions

D.A. and S.H.-B. designed the experiments. D.A. performed the experiments and analyzed data. D.A. and S.H.-B. prepared figures and wrote the manuscript.

Funding

This work was supported by the American Cancer Society [RSG-14-176 to S.H.-B.]; and the National Institutes of Health [R01GM094276 to S.H.-B.]. Deposited in PMC for release after 12 months.

Supplementary information

Supplementary information available online at
http://dev.biologists.org/lookup/suppl/doi:10.1242/dev.131276/-/DC1

References

Allikian, M. J., Bhabha, G., Dospoy, P., Heydemann, A., Ryder, P., Earley, J. U., Wolf, M. J., Rockman, H. A. and McNally, E. M. (2007). Reduced life span with heart and muscle dysfunction in Drosophila sarcoglycan mutants. *Hum. Mol. Genet.* **16**, 2933-2943.

Bownes, M. (1982). Hormonal and genetic regulation of vitellogenesis in Drosophila. *Q. Rev. Biol.* **57**, 247-274.

Bownes, M. and Hames, B. D. (1978). Genetic analysis of vitellogenesis in Drosophila melanogaster: the identification of a temperature-sensitive mutation affecting one of the yolk proteins. *J. Embryol. Exp. Morphol.* **47**, 111-120.

Buszczak, M., Paterno, S., Lighthouse, D., Bachman, J., Planck, J., Owen, S., Skora, A. D., Nystul, T. G., Ohlstein, B., Allen, A. et al. (2007). The carnegie protein trap library: a versatile tool for Drosophila developmental studies. *Genetics* **175**, 1505-1531.

Butterworth, F. M., Burde, V. S. and Bownes, M. (1992). Mutant yolk proteins lead to female sterility in Drosophila. *Dev. Biol.* **154**, 182-194.

Cant, K. and Cooley, L. (1996). Single amino acid mutations in Drosophila fascin disrupt actin bundling function in vivo. *Genetics* **143**, 249-258.

Cetera, M., Ramirez-San Juan, G. R., Oakes, P. W., Lewellyn, L., Fairchild, M. J., Tanentzapf, G., Gardel, M. L. and Horne-Badovinac, S. (2014). Epithelial rotation promotes the global alignment of contractile actin bundles during Drosophila egg chamber elongation. *Nat. Commun.* **5**, 5511.

Cook, B. J. and Peterson, T. (1989). Ovarian muscularis of the stable fly Stomoxys calcitrans: its structural, motile, and pharmacological properties. *Arch. Insect Biochem.* **12**, 15-30.

Cruickshank, W. (1973). The ultrastructure and functions of the ovariole sheath and tunica propria in the flour moth. *J. Insect Physiol.* **19**, 577-592.

Cullen, M. J. and Fulthorpe, J. J. (1975). Stages in fibre breakdown in Duchenne muscular dystrophy. An electron-microscopic study. *J. Neurol. Sci.* **24**, 179-200.

Cummings, M. R. (1974). Ultrastructure of ovarian epithelial sheath in Drosophila melanogaster meigen (Diptera: Drosophilidae). *Int. J. Insect Morphol. Embryol.* **3**, 137-145.

Delon, I. and Brown, N. H. (2009). The integrin adhesion complex changes its composition and function during morphogenesis of an epithelium. *J. Cell Sci.* **122**, 4363-4374.

Deng, W.-M., Schneider, M., Frock, R., Castillejo-Lopez, C., Gaman, E. A., Baumgartner, S. and Ruohola-Baker, H. (2003). Dystroglycan is required for polarizing the epithelial cells and the oocyte in Drosophila. *Development* **130**, 173-184.

Dialynas, G., Speese, S., Budnik, V., Geyer, P. K. and Wallrath, L. L. (2010). The role of Drosophila Lamin C in muscle function and gene expression. *Development* **137**, 3067-3077.

DiMario, P. J. and Mahowald, A. P. (1987). Female sterile (1) yolkless: a recessive female sterile mutation in Drosophila melanogaster with depressed numbers of coated pits and coated vesicles within the developing oocytes. *J. Cell Biol.* **105**, 199-206.

Duffy, J. B., Harrison, D. A. and Perrimon, N. (1998). Identifying loci required for follicular patterning using directed mosaics. *Development* **125**, 2263-2271.

Ervasti, J. M. and Sonnemann, K. J. (2008). Biology of the striated muscle dystrophin-glycoprotein complex. *Int. Rev. Cytol.* **265**, 191-225.

Frydman, H. M. and Spradling, A. C. (2001). The receptor-like tyrosine phosphatase lar is required for epithelial planar polarity and for axis determination within drosophila ovarian follicles. *Development* **128**, 3209-3220.

Gates, J. (2012). Drosophila egg chamber elongation: insights into how tissues and organs are shaped. *Fly* **6**, 213-227.

Gupta, V. A., Kawahara, G., Myers, J. A., Chen, A. T., Hall, T. E., Manzini, M. C., Currie, P. D., Zhou, Y., Zon, L. I., Kunkel, L. M. et al. (2012). A splice site mutation in laminin-alpha2 results in a severe muscular dystrophy and growth abnormalities in zebrafish. *PLoS ONE* **7**, e43794.

Gutzeit, H. O. and Haas-Assenbaum, A. (1991). The somatic envelopes around the germ-line cells of polytrophic insect follicles: structural and functional aspects. *Tissue Cell* **23**, 853-865.

Haigo, S. L. and Bilder, D. (2011). Global tissue revolutions in a morphogenetic movement controlling elongation. *Science* **331**, 1071-1074.

Haines, N., Seabrooke, S. and Stewart, B. A. (2007). Dystroglycan and protein O-mannosyltransferases 1 and 2 are required to maintain integrity of Drosophila larval muscles. *Mol. Biol. Cell* **18**, 4721-4730.

Hames, B. D. and Bownes, M. (1978). Synthesis of yolk proteins in Drosophila melanogaster. *Insect Biochem.* **8**, 319-328.

Holmberg, J. and Durbeej, M. (2013). Laminin-211 in skeletal muscle function. *Cell. Adh. Migr.* **7**, 111-121.

Horne-Badovinac, S. (2014). The Drosophila egg chamber–a new spin on how tissues elongate. *Integr. Comp. Biol.* **54**, 667-676.

Hudson, A. M., Petrella, L. N., Tanaka, A. J. and Cooley, L. (2008). Mononuclear muscle cells in Drosophila ovaries revealed by GFP protein traps. *Dev. Biol.* **314**, 329-340.

Irizarry, J. and Stathopoulos, A. (2015). FGF signaling supports Drosophila fertility by regulating development of ovarian muscle tissues. *Dev. Biol.* **404**, 1-13.

Lin, H. and Spradling, A. C. (1993). Germline stem cell division and egg chamber development in transplanted Drosophila germaria. *Dev. Biol.* **159**, 140-152.

Martin, D., Zusman, S., Li, X., Williams, E. L., Khare, N., DaRocha, S., Chiquet-Ehrismann, R. and Baumgartner, S. (1999). wing blister, a new Drosophila

laminin alpha chain required for cell adhesion and migration during embryonic and imaginal development. *J. Cell Biol.* **145**, 191-201.

McGuire, S. E., Mao, Z. and Davis, R. L. (2004). Spatiotemporal gene expression targeting with the TARGET and gene-switch systems in Drosophila. *Sci. STKE* **2004**, pl6.

Middleton, C. A., Nongthomba, U., Parry, K., Sweeney, S. T., Sparrow, J. C. and Elliott, C. J. H. (2006). Neuromuscular organization and aminergic modulation of contractions in the Drosophila ovary. *BMC Biol.* **4**, 17.

Miller, A. (1950). The internal anatomy and histology of the imago of Drosophila melanogaster. In *Biology of Drosophila* (ed. M. Demerec), pp. 420-534. New York, USA: Cold Spring Harbor Laboratory Press.

Ozawa, E., Nishino, I. and Nonaka, I. (2001). Sarcolemmopathy: muscular dystrophies with cell membrane defects. *Brain Pathol.* **11**, 218-230.

Pass, G. (2000). Accessory pulsatile organs: evolutionary innovations in insects. *Annu. Rev. Entomol.* **45**, 495-518.

Plantié, E., Migocka-Patrzałek, M., Daczewska, M. and Jagla, K. (2015). Model organisms in the fight against muscular dystrophy: lessons from drosophila and Zebrafish. *Molecules* **20**, 6237-6253.

Prasad, M., Jang, A.-C., Starz-Gaiano, M., Melani, M. and Montell, D. J. (2007). A protocol for culturing Drosophila melanogaster stage 9 egg chambers for live imaging. *Nat. Protoc.* **2**, 2467-2473.

Ranganayakulu, G., Zhao, B., Dokidis, A., Molkentin, J. D., Olson, E. N. and Schulz, R. A. (1995). A series of mutations in the D-MEF2 transcription factor reveal multiple functions in larval and adult myogenesis in Drosophila. *Dev. Biol.* **171**, 169-181.

Ranganayakulu, G., Elliott, D. A., Harvey, R. P. and Olson, E. N. (1998). Divergent roles for NK-2 class homeobox genes in cardiogenesis in flies and mice. *Development* **125**, 3037-3048.

Rittenhouse, K. R. and Berg, C. A. (1995). Mutations in the Drosophila gene bullwinkle cause the formation of abnormal eggshell structures and bicaudal embryos. *Development* **121**, 3023-3033.

Robinson, D. N. and Cooley, L. (1997). Genetic analysis of the actin cytoskeleton in the Drosophila ovary. *Annu. Rev. Cell Dev. Biol.* **13**, 147-170.

Schneider, M., Khalil, A. A., Poulton, J., Castillejo-Lopez, C., Egger-Adam, D., Wodarz, A., Deng, W.-M. and Baumgartner, S. (2006). Perlecan and Dystroglycan act at the basal side of the Drosophila follicular epithelium to maintain epithelial organization. *Development* **133**, 3805-3815.

Shcherbata, H. R., Yatsenko, A. S., Patterson, L., Sood, V. D., Nudel, U., Yaffe, D., Baker, D. and Ruohola-Baker, H. (2007). Dissecting muscle and neuronal disorders in a Drosophila model of muscular dystrophy. *EMBO J.* **26**, 481-493.

Srdic, Z. and Jacobs-Lorena, M. (1978). Drosophila egg chambers develop to mature eggs when cultured in vivo. *Science* **202**, 641-643.

Tögel, M., Pass, G. and Paululat, A. (2008). The Drosophila wing hearts originate from pericardial cells and are essential for wing maturation. *Dev. Biol.* **318**, 29-37.

Trougakos, I. P., Papassideri, I. S., Waring, G. L. and Margaritis, L. H. (2001). Differential sorting of constitutively co-secreted proteins in the ovarian follicle cells of Drosophila. *Eur. J. Cell Biol.* **80**, 271-284.

Wallace, G. Q. and McNally, E. M. (2009). Mechanisms of muscle degeneration, regeneration, and repair in the muscular dystrophies. *Annu. Rev. Physiol.* **71**, 37-57.

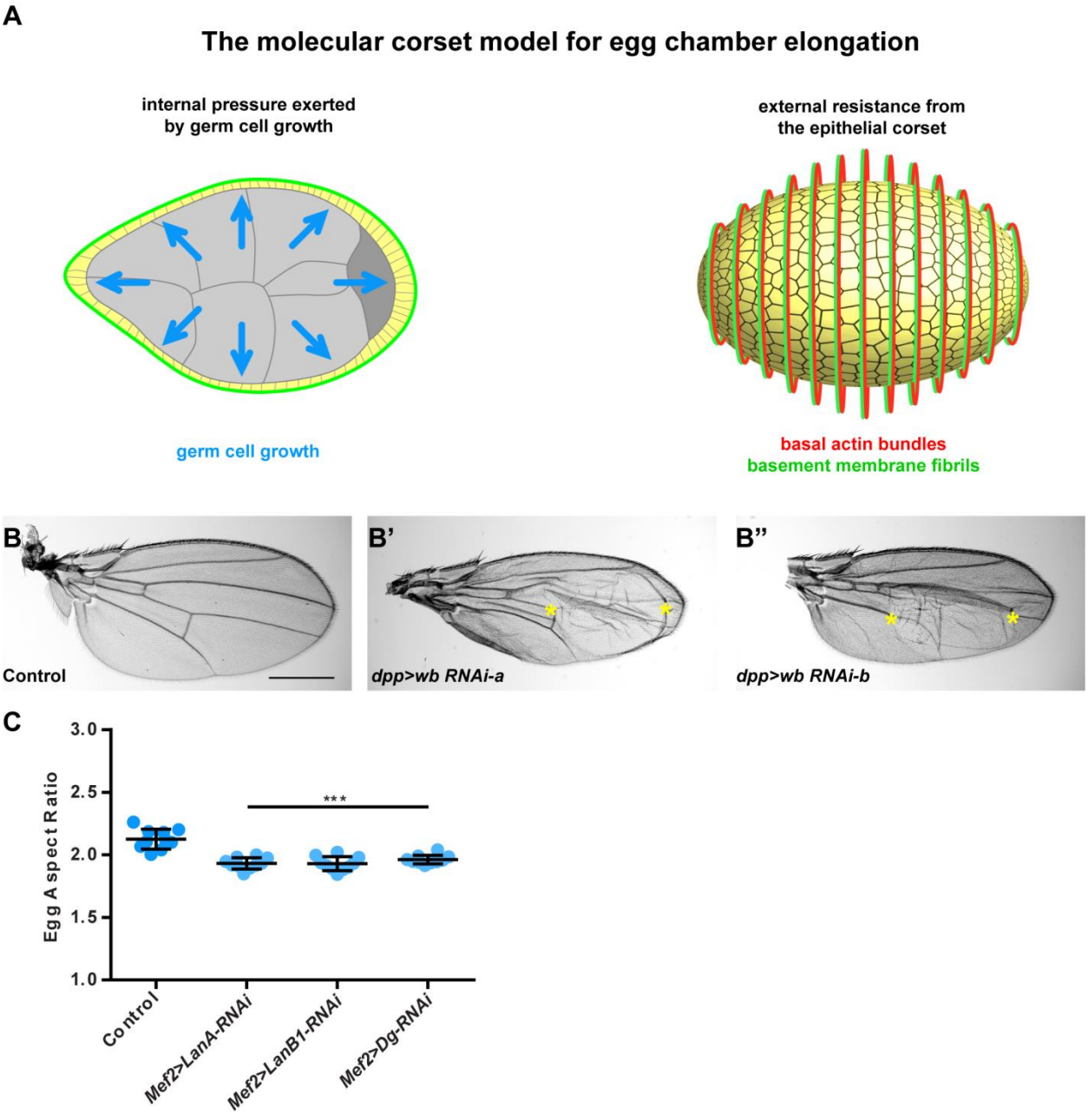

Figure S1. *wb-RNAi* validation and depletion of LanA, LanB1 & Dg with *Mef2-Gal4*

(A) Overview of the molecular corset model for egg chamber elongation. (B) Both *wb-RNAi* transgenes used in this study produce blisters in adult wings (yellow stars) when driven with *decapentaplegic-Gal4* (*dpp-Gal4*). Scale bar = 500 µm. (C) Using *Mef2-Gal4* to deplete LanA, LanB1 or Dg from the muscle sheath reduces the egg's aspect ratio. Data represent mean ± s.d., *t*-test *** = P<0.001. n = 9-10 eggs per condition.

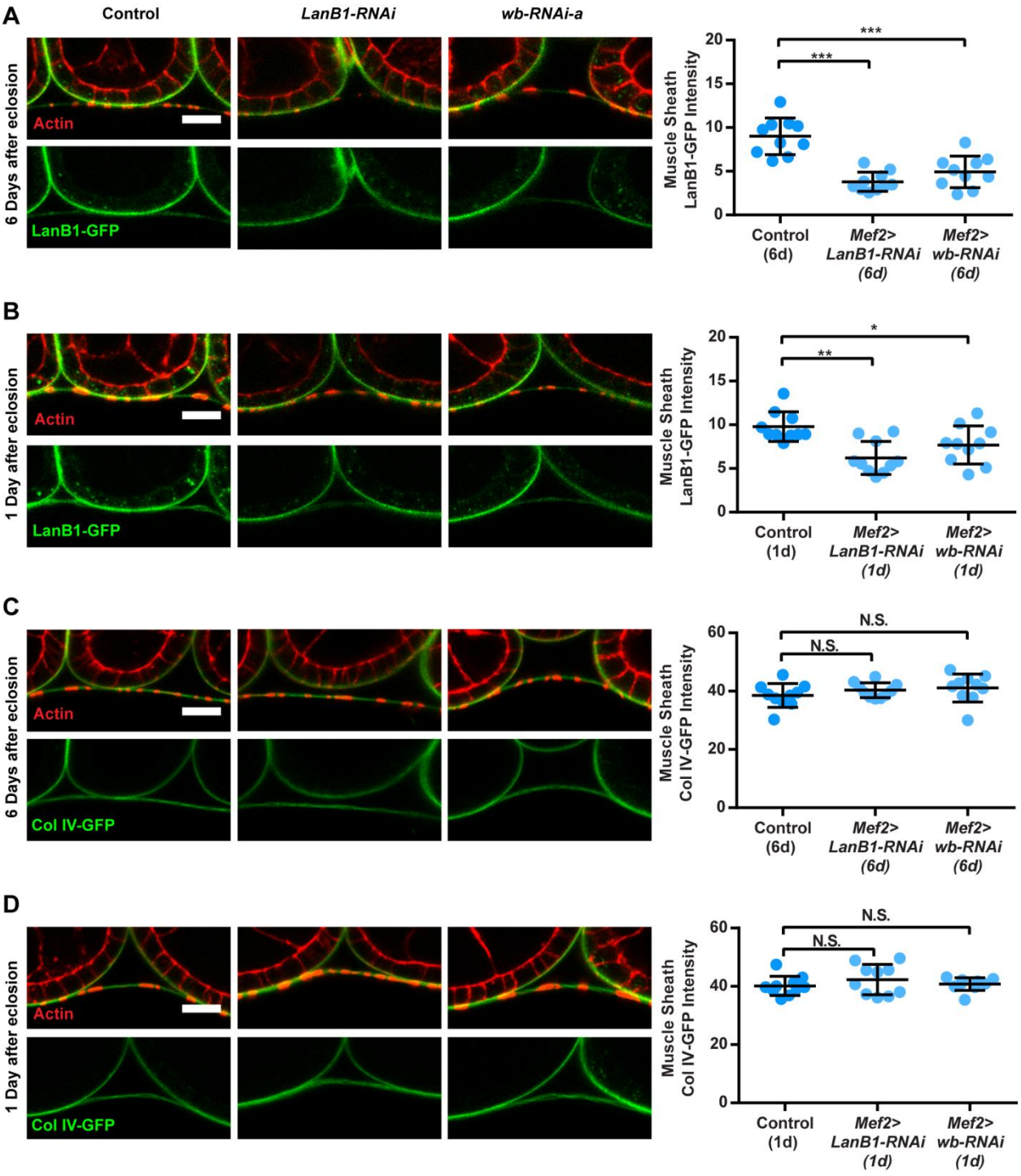

Figure S2. *Mef2>LanB1-RNAi and Mef2>wb-RNAi-a* both reduce Laminin levels in muscle sheath BMs, without disrupting Col IV levels

(A-B) *Mef2>LanB1-RNAi and Mef2>wb-RNAi-a* both reduce Laminin levels in muscle sheath BMs. Laminin levels are monitored using 1 copy of a *LanB1-GFP* fosmid transgene, where LanB1 is expressed under its endogenous promoter. Both RNAi transgenes reduce LanB1-GFP levels compared to controls; however, the effect is stronger for *LanB1-RNAi* than for *wb-RNAi*. This difference is expected, as LamininA and LamininW both appear to be expressed in the muscle sheath, and LanB1 is a subunit of both isoforms, whereas Wb is only a subunit of one. The reduction in LanB1-GFP is also higher for both RNAi transgenes 6 days after eclosion (A) compared to 1 day after eclosion (B). (C-D) In contrast, the same set of RNAi conditions has no effect on the levels of the other major BM protein, Collagen IV. Collagen IV levels are monitored using one copy of a GFP protein trap in the Collagen IV α2 chain Viking. (A-D) Data represent mean ± s.d., *t*-test * = P<0.05, ** = P<0.01, *** = P<0.001. n = 10 ovarioles per condition.

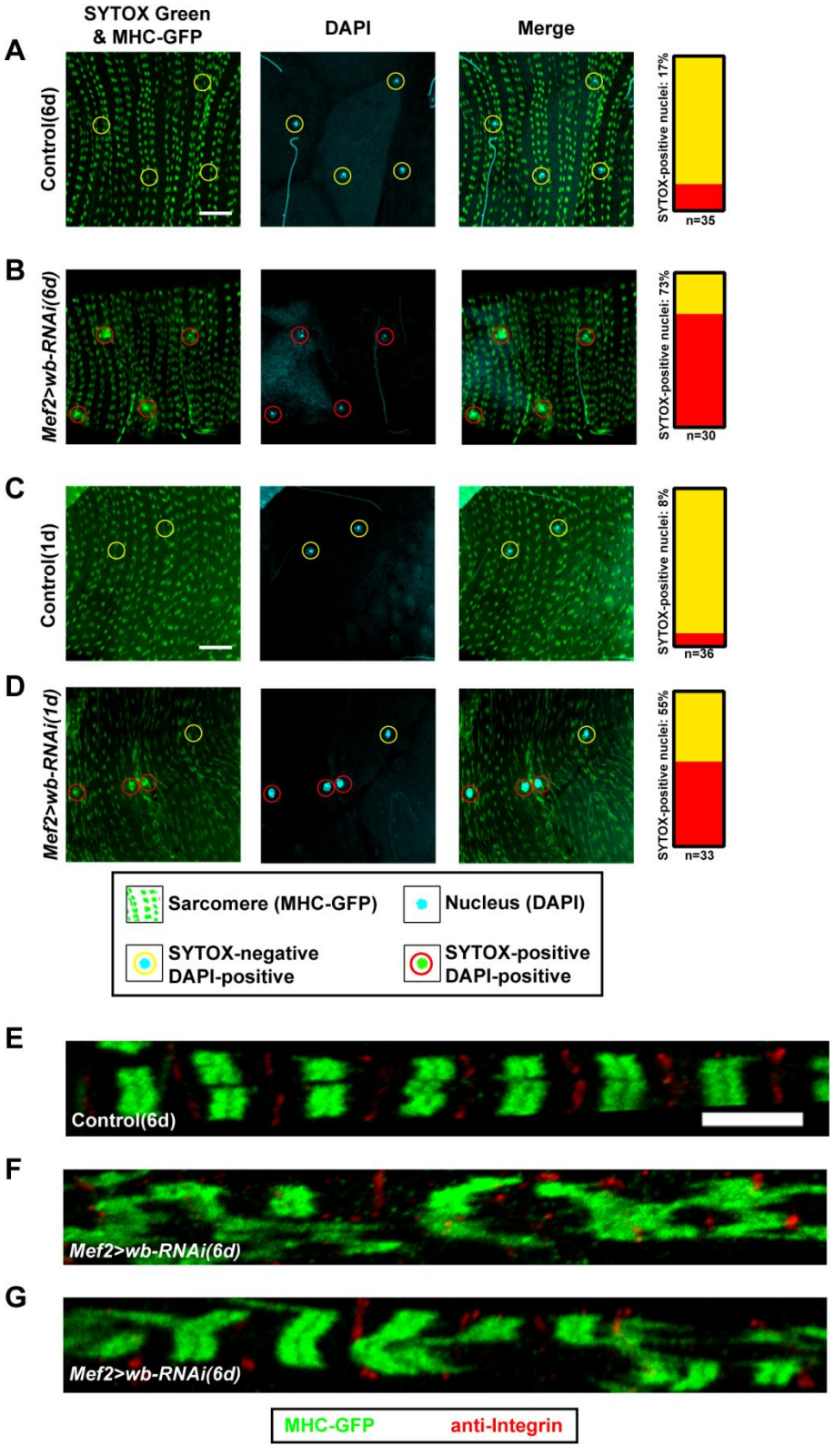

Figure S3. Wb depletion causes damage to the muscle sheath

(A-D) SYTOX Green labelling of muscle sheath nuclei identifies cells whose plasma membranes have been breached. Representative images showing the muscle sheath sarcomeres labelled with Myosin Heavy Chain GFP (MHC-GFP) and muscle sheath nuclei labelled with DAPI. Nuclei that are co-labelled with SYTOX Green are circled in red and those that lack SYTOX green are circled in yellow. Scale bars = 20 µm. Graphs show the percentage of labelled nuclei for each condition. Increased labelling is seen under both *Mef2>wb-RNAi(6d)* (A-B) and *Mef2>wb-RNAi(1d)* (C-D). (E-G) Micrographs showing the sarcomeric structure of the muscle sheath. MHC-GFP marks the A-band (green) and anti-integrin-βPS marks the Z-discs (red). (E) Image showing normal sarcomere structure in a control muscle sheath. Scale bar = 5 µm. (F,G) Under *Mef2>wb-RNAi(6d)* the muscle fibers begin to tear and sarcomeres become highly disorganized.

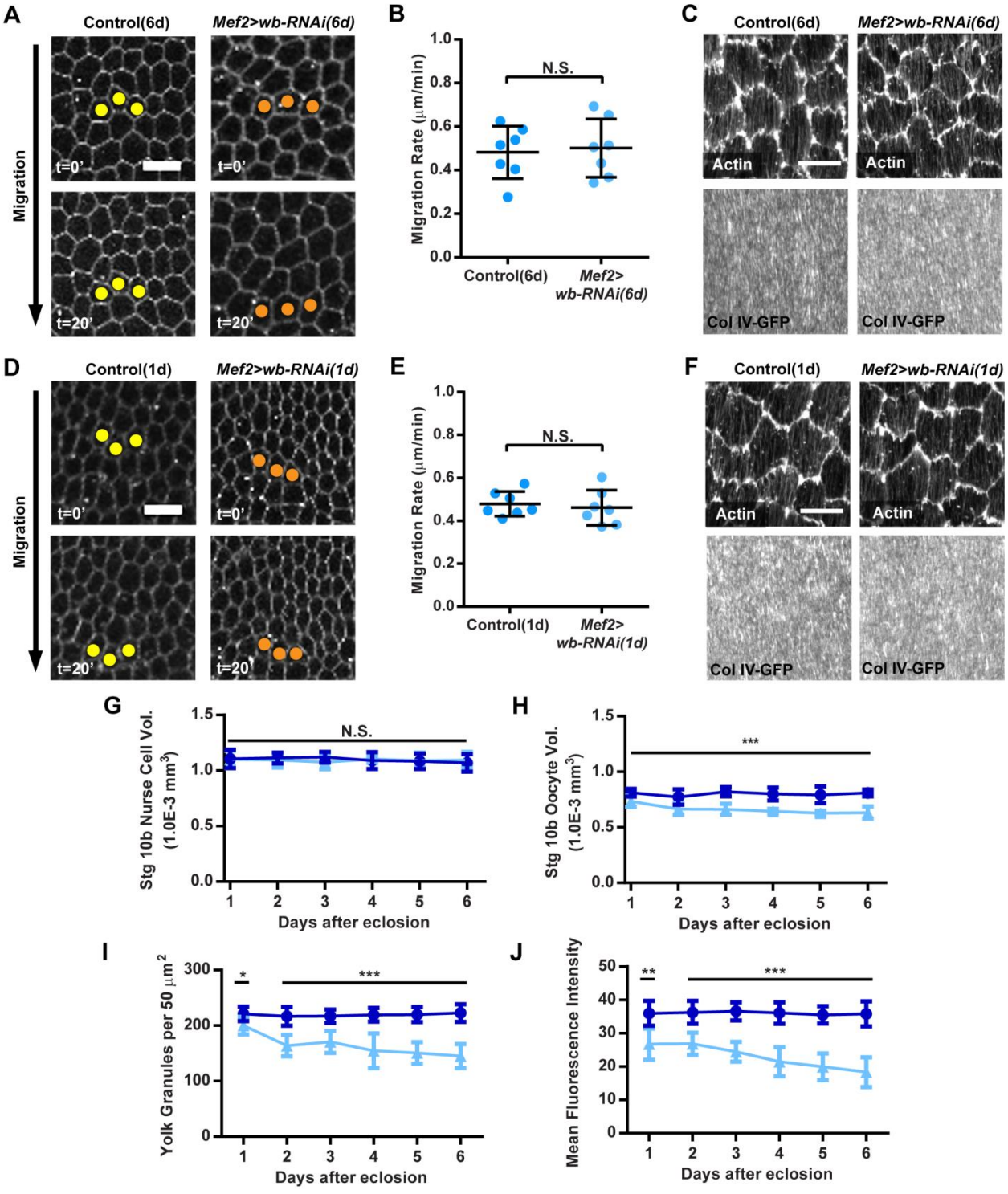

Figure S4. Effect of *Mef2>wb-RNAi* on the molecular corset & vitellogenesis time course

(A-F) The molecular corset in the follicular epithelium is normal in stage 7 egg chambers under both the *Mef2>wb-RNAi(6d)* and *Mef2>wb-RNAi(1d)* conditions. (A,D) Stills from representative movies showing that the follicle cells migrate normally under *Mef2>wb-RNAi*. Colored dots mark the same three cells between the two time points for each condition. (B,E) Graphs quantifying the effects shown in (A,D). (C,F) Representative images of the basal actin bundles and polarized basement membrane showing that their organization is unaffected by *Mef2>wb-RNAi.* The actin bundles are marked with rhodamine-phalloidin and the basement membrane with a GFP protein trap in the Collagen IV α2 chain Viking. (A,C,D,F) Scale bars = 10 μm. (G-J) A time-course experiment shows that Wb depletion from the muscle sheath causes an increasing defect in vitellogenesis over time. Wb was depleted from the muscle sheath and four phenotypes were measured in stage 10b egg chambers each day for six days: (G) nurse cell volume, (H) oocyte volume, (I) yolk granule density and (J) yolk granule auto-fluorescence. (G-J) All values except nurse cell volume decrease over time. Data represent mean ± s.d., *t*-test * = P<0.05, ** = P<0.01, *** = P<0.001. n = 10 egg chambers per condition per day.

Movie 1. *Mef2>wb-RNAi(6d)* largely eliminates ovarian contractions

Movie showing the contractile activity of a single cultured ovary from either a Control(6d) (left) or *Mef2>wb-RNAi(6d)* (right) female. Length = 1 min.

Movie 2. *Mef2>wb-RNAi(6d)* does not affect egg chamber rotation

Movie showing that rotation occurs normally in stage 7 egg chambers from both Control(6d) (left) and *Mef2>wb-RNAi(6d)* (right) females. Cell membranes are marked with CellMask. Laser-scanning confocal images. Length = 20 min/ 1 min intervals. Scale bar = 20 μm.

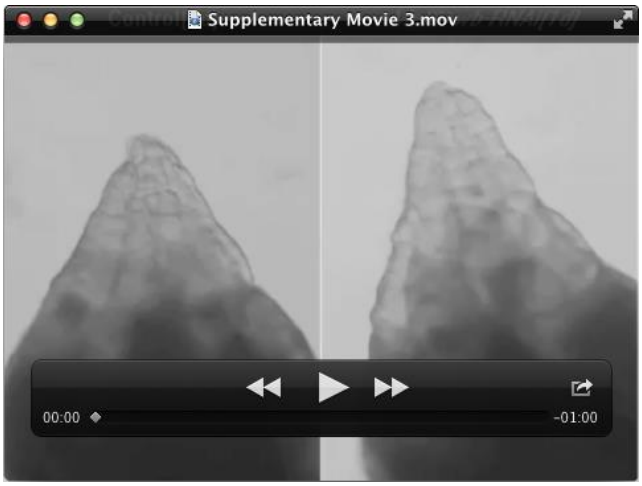

Movie 3. *Mef2>wb-RNAi(1d)* increases the frequency of ovarian contractions

Movie showing the contractile activity of a single cultured ovary from either a Control(1d) (left) or *Mef2>wb-RNAi(1d)* (right) female. Length = 1 min.

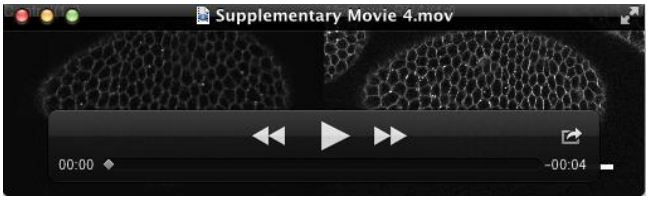

Movie 4. *Mef2>wb-RNAi(1d)* does not affect egg chamber rotation

Movie showing that rotation occurs normally in stage 7 egg chambers from both Control(1d) (left) and *Mef2>wb-RNAi(1d)* (right) females. Cell membranes are marked with CellMask. Laser-scanning confocal images. Length = 20 min/ 1 min intervals. Scale bar = 20 μm.

SUPPLEMENTARY MATERIALS AND METHODS

Measurements of BM protein levels in the muscle sheath

Ovaries were fixed and stained with phalloidin, and images were taken of central transverse sections through isolated ovarioles. In ImageJ, lines with a width of 10 pixels were then drawn over regions of the muscle sheath that were not in contact with an egg chamber, and the mean fluorescence intensity of either Col IV-GFP or LanB1-GFP was measured along those lines. At least four measurements of this type were made for each ovariole. These values were then averaged and displayed as a single data point. Confocal settings were held constant for all experiments with a given GFP transgene.

Measurement of egg chamber rotation rates

Ovaries were dissected in live imaging media as described (Prasad et al., 2007). CellMask dye (1:1000, Thermofisher) was added to the live imaging media to mark cell membranes. Ovarioles were transferred in live imaging media + CellMask to an agar pad (live imaging media with 0.4% NuSieve GTG low-melt agarose) that was formed on a gas permeable membrane slide (Sarstedt Inc, catalog # 94.6150.101). Most of the live imaging media was removed from the pad and a coverslip was placed on top of the sample, stabilized with vacuum grease at each corner. The coverslip was then gently compressed onto the sample and halocarbon oil 27 (Sigma) was added around the coverslip to keep the media from evaporating. Egg chambers were imaged with a 40/1.3 numerical aperture (NA) EC Plan-NeoFluor oil-immersion objective on a laser-scanning confocal microscope (Zeiss LSM510) controlled by the LSM acquisition software. ImageJ was used for image processing. To determine rotation rates, kymographs were generated from movies of rotating egg chambers, and the migration rate was measured as the slope of lines corresponding to cell membranes moving over time.

SYTOX Green staining

Freshly dissected ovaries were incubated in S2 media with SYTOX Green (1:5000, Invitrogen) and DAPI (1:1000, Sigma) for 15 minutes, washed with PBS, and fixed for 15 minutes in PBS + formaldehyde. Ovarioles were separated with forceps and mounted in antifade. Images were taken of muscle sheath overlaying stage 10 egg chambers for quantification of labelled nuclei, with confocal settings held constant among all conditions.

Hemolymph collection and processing

A hemolymph collection chamber was fabricated using a 20 gauge needle to make four holes in the base of a 0.5 mL microcentrifuge tube, and then placing that tube inside a 1.5 mL microcentrifuge tube. A 33 gauge needle was then used to puncture the dorsal thorax of four adult females, which were loaded into the smaller tube and centrifuged at 4°C for 5 minutes at 5600 rpm. The smaller tube was discarded and 2 µL of hemolymph buffer (S2 media + protease inhibitor cocktail (1:100, Sigma p2714) was added to the hemolymph in the larger tube. To dilute this sample, 1 µL was added to a new tube containing 8 µL of hemolymph buffer. 1.33 µL of this dilution was then added to a new tube containing 8 µL of hemolymph buffer and 8 µL of SDS-Page sample buffer.

Table S1 References for RNAi transgenes

RNAi transgene	Reference
UAS-wb-RNAi$^{TRiP.JF03238}$	(Papagiannouli et al., 2014)
UAS-wb-RNAi^{v108020}	(Kim and Choe, 2014) (Han et al., 2012)
UAS-LanA-RNAi$^{TRiP.JF02908}$	(Papagiannouli et al., 2014) (Kim and Choe, 2014)
UAS-LanB1-RNAi^{v23121}	(Kim and Choe, 2014)
UAS-Dg-RNAi^{v107029}	(Kim and Choe, 2014)

Table S2 Detailed experimental genotypes and conditions

Fig.	Panel	Genotype	Temp for cross	Females on yeast	
				Temp	No. days
2	B	*tj-Gal4/ +; UAS-mCD8-GFP/ +*	25°C	25°C	2
	C	*tj-Gal4/ +*	RT	29°C	6
		tj-Gal4/ +; UAS-wb-RNAi$^{TRiP.JF03238}$	RT	29°C	6
		tj-Gal4/ UAS-wb-RNAi^{v108020}	RT	29°C	6
	D	*Mef2-Gal4/ UAS-mCD8-GFP*	25°C	25°C	2
	E	*Mef2-Gal4/ +*	RT	29°C	6
		Mef2-Gal4/ UAS-wb-RNAi$^{TRiP.JF03238}$	RT	29°C	6
		TubP-Gal80^{ts}/ +; Mef2-Gal4/ +	18°C	29°C	6
		TubP-Gal80^{ts}/ UAS-wb-RNAi^{v108020}; Mef2-Gal4/ +	18°C	29°C	6
	F	*tj-Gal4, Mef2-Gal80/ +; UAS-mCD8-GFP/ +*	25°C	25°C	2
	G	*tj-Gal4, Mef2-Gal80/ +*	RT	29°C	6
		tj-Gal4, Mef2-Gal80/ +; UAS-LanA-RNAi$^{TRiP.JF02908}$	RT	29°C	6
		tj-Gal4, Mef2-Gal80/ +; UAS-wb-RNAi$^{TRiP.JF03238}$	RT	29°C	6
3	B C	*MHC-GFP/ +; Mef2-Gal4/ +*	RT	29°C	5
		MHC-GFP/ +; Mef2-Gal4/ UAS-wb-RNAi$^{TRiP.JF03238}$	RT	29°C	5
	D	*Mef2-Gal4/ +*	RT	29°C	6
	E F	*Mef2-Gal4/ +*	RT	29°C	6
		Mef2-Gal4/ UAS-wb-RNAi$^{TRiP.JF03238}$	RT	29°C	6
4	A-F	*Mef2-Gal4/ +*	RT	29°C	6
		Mef2-Gal4/ UAS-wb-RNAi$^{TRiP.JF03238}$	RT	29°C	6
5	A-C	*Mef2-Gal4/ +*	RT	29°C	6
		Mef2-Gal4/ UAS-wb-RNAi$^{TRiP.JF03238}$	RT	29°C	6
	D-G	*w^{1118}*	RT	29°C	1
		Yp1^{ts}/ Df(1)C52	RT	29°C	1
6	B-E	*vkg-GFP*	25°C	25°C	3
		Host: Ovo^{D1} v^{24}/ + Donor: vkg-GFP	25°C	25°C	3
7	A-C	*w^{1118}*	RT	25°C	1
		sn^{G409E}	RT	25°C	1
		bwk^{151}/bwk^{08482}	RT	25°C	1
8	A	*Mef2-Gal4/ +*	RT	29°C	1-7
		Mef2-Gal4/ UAS-wb-RNAi$^{TRiP.JF03238}$	RT	29°C	1-7
	B	*Mef2-Gal4/ +*	RT	29°C	1-7
		UAS-Dg-RNAi^{v107029}/ +; Mef2-Gal4/ +	RT	29°C	1-7
	C D	*MHC-GFP/ +; Mef2-Gal4/ +*	RT	29°C	1
		MHC-GFP/ +; Mef2-Gal4/ UAS-wb-RNAi$^{TRiP.JF03238}$	RT	29°C	1
	E	*Mef2-Gal4/ +*	RT	29°C	1

	F G	*Mef2-Gal4/ +*	RT	29°C	1
		Mef2-Gal4/ UAS-wb-RNAi$^{TRiP.JF03238}$	RT	29°C	1
9	A-E H J	*Mef2-Gal4/ +*	RT	29°C	1
		Mef2-Gal4/ UAS-wb-RNAi$^{TRiP.JF03238}$	RT	29°C	1
	G I	*Mef2-Gal4/ +*	RT	29°C	6
		Mef2-Gal4/ UAS-wb-RNAi$^{TRiP.JF03238}$	RT	29°C	6
S1	B	*dpp-Gal4/ +*	25°C	25°C	3
		dpp-Gal4/ UAS-wb-RNAi$^{TRiP.JF03238}$	25°C	25°C	3
		UAS-wb-RNAi^{v108020}/ +; dpp-Gal4/+	25°C	25°C	3
	C	*Mef2-Gal4/ +*	RT	29°C	6
		Mef2-Gal4/ UAS-LanA-RNAi$^{TRiP.JF02908}$	RT	29°C	6
		Mef2-Gal4/ UAS-LanB1-RNAi^{v23121}	RT	29°C	6
		UAS-Dg-RNAi^{v107029}/ +; Mef2-Gal4/ +	RT	29°C	6
S2	A	*Mef2-Gal4, LanB1-GFP/ +*	RT	29°C	6
		Mef2-Gal4, LanB1-GFP/UAS-LanB1-RNAi^{v23121}	RT	29°C	6
		Mef2-Gal4, LanB1-GFP/ UAS-wb-RNAi$^{TRiP.JF03238}$	RT	29°C	6
	B	*Mef2-Gal4, LanB1-GFP/ +*	RT	29°C	1
		Mef2-Gal4, LanB1-GFP/UAS-LanB1-RNAi^{v23121}	RT	29°C	1
		Mef2-Gal4, LanB1-GFP/ UAS-wb-RNAi$^{TRiP.JF03238}$	RT	29°C	1
	C	*vkg-GFP/ +; Mef2-Gal4/ +*	RT	29°C	6
		vkg-GFP/ +; Mef2-Gal4/ UAS-LanB1-RNAi^{v23121}	RT	29°C	6
		vkg-GFP/ +; Mef2-Gal4/ UAS-wb-RNAi$^{TRiP.JF03238}$	RT	29°C	6
	D	*vkg-GFP/ +; Mef2-Gal4/ +*	RT	29°C	1
		vkg-GFP/ +; Mef2-Gal4/ UAS-LanB1-RNAi^{v23121}	RT	29°C	1
		vkg-GFP/ +; Mef2-Gal4/ UAS-wb-RNAi$^{TRiP.JF03238}$	RT	29°C	1
S3	A E	*MHC-GFP/+; Mef2-Gal4/ +*	RT	29°C	6
	B F G	*MHC-GFP/+; Mef2-Gal4/ UAS-wb-RNAi$^{TRiP.JF03238}$*	RT	29°C	6
	C	*MHC-GFP/+; Mef2-Gal4/ +*	RT	29°C	1
	D	*MHC-GFP/+; Mef2-Gal4/ UAS-wb-RNAi$^{TRiP.JF03238}$*	RT	29°C	1
S4	A B	*Mef2-Gal4/ +*	RT	29°C	6
		Mef2-Gal4/ UAS-wb-RNAi$^{TRiP.JF03238}$	RT	29°C	6
	C	*vkg-GFP/ +; Mef2-Gal4/ +*	RT	29°C	6
		vkg-GFP/ +; Mef2-Gal4/ UAS-wb-RNAi$^{TRiP.JF03238}$	RT	29°C	6
	D E	*Mef2-Gal4/ +*	RT	29°C	1
		Mef2-Gal4/ UAS-wb-RNAi$^{TRiP.JF03238}$	RT	29°C	1
	F	*vkg-GFP/ +; Mef2-Gal4/ +*	RT	29°C	1
		vkg-GFP/ +; Mef2-Gal4/ UAS-wb-RNAi$^{TRiP.JF03238}$	RT	29°C	1
	G-J	*Mef2-Gal4/ +*	RT	29°C	1-6
		Mef2-Gal4/ UAS-wb-RNAi$^{TRiP.JF03238}$	RT	29°C	1-6

SUPPLEMENTARY REFERENCES

Han, C., Wang, D., Soba, P., Zhu, S., Lin, X., Jan, L. Y. and Jan, Y. N. (2012). Integrins regulate repulsion-mediated dendritic patterning of drosophila sensory neurons by restricting dendrites in a 2D space. *Neuron* **73**, 64-78.

Kim, M. J. and Choe, K. M. (2014). Basement membrane and cell integrity of self-tissues in maintaining Drosophila immunological tolerance. *PLoS Genet* **10**, e1004683.

Papagiannouli, F., Schardt, L., Grajcarek, J., Ha, N. and Lohmann, I. (2014). The Hox gene Abd-B controls stem cell niche function in the Drosophila testis. *Dev Cell* **28**, 189-202.

Prasad, M., Jang, A. C., Starz-Gaiano, M., Melani, M. and Montell, D. J. (2007). A protocol for culturing Drosophila melanogaster stage 9 egg chambers for live imaging. *Nat Protoc* **2**, 2467-2473.